Journal of Medicinal Chemistry

Article

Discovery of a new inhibitor of myeloid differentiation 2 from cinnamamide derivatives with anti-inflammatory activity in sepsis and acute lung injury

Gaozhi Chen, Yali Zhang, Xing Liu, Qilu Fang, Zhe Wang, Lili Fu, Zhiguo Liu, Yi Wang, Yunjie Zhao, Xiaokun Li, and Guang Liang

J. Med. Chem., **Just Accepted Manuscript** • DOI: 10.1021/acs.jmedchem.5b01574 • Publication Date (Web): 03 Mar 2016

ACS Publications

Journal of Medicinal Chemistry is published by the American Chemical Society. 1155 Sixteenth Street N.W., Washington, DC 20036

Discovery of a new inhibitor of myeloid differentiation 2 from cinnamamide derivatives with anti-inflammatory activity in sepsis and acute lung injury

Gaozhi Chen, Yali Zhang, Xing Liu, Qilu Fang, Zhe Wang, Lili Fu, Zhiguo Liu, Yi Wang, Yunjie Zhao, Xiaokun Li, Guang Liang*

Chemical Biology Research Center, School of Pharmaceutical Sciences, Wenzhou Medical University, Wenzhou, Zhejiang 325035, China

* Corresponding authors:

Guang Liang, Ph.D, Professor

Director, Chemical Biology Research Center

School of Pharmaceutical Sciences, Wenzhou Medical University

Tel: (+86)-577-86699396; Fax: (+86)-577-86699396

E-mail: wzmcliangguang@163.com

Abstract: Acute inflammatory diseases, including acute lung injury and sepsis, remain the most common life-threatening illness in ICU worldwide. Cinnamamide has been incorporated in several synthetic compounds with therapeutic potentials including anti-inflammatory properties. However, the possible mechanism and direct molecular target of cinnamamides for their anti-inflammatory effects were rarely investigated. In this study, we synthesized a series of cinnamamides and evaluated their anti-inflammatory activities. The most active compound, 2i, was found to block LPS-induced MD2/TLR4 pro-inflammatory signaling activation *in vitro* and to attenuate LPS-caused sepsis and acute lung injury *in vivo*. Mechanistically, we demonstrated that 2i exerts its anti-inflammatory effects by directly targeting and binding MD2 in Arg90 and Tyr102 residues and inhibiting MD2/TLR4 complex formation. Taken together, this work presents a novel MD2 inhibitor, 2i, which has the potential to be developed as a candidate for the treatment of sepsis, and provides a new lead structure for the development of anti-inflammatory agents targeting MD2.

Keywords: Acute inflammatory diseases, Cinnamanides, MD2, TLR4, Acute lung injury

Introduction

Acute inflammatory diseases such as acute lung injury (ALI) and sepsis, which occur as a result of local or systemic inflammation, remain the most common cause of death in intensive care units worldwide[1]. Lipopolysaccharide (LPS) is a main stimulator of the acute inflammation that leads to sepsis and ALI[2]. Microbial LPS binds to a surface receptor complex consisting of myeloid differentiation 2 (MD2) and toll-like receptor 4 (TLR4) in innate immune cells through ancillary proteins such as LPS-binding protein (LBP) and cluster of differentiation 14 (CD14)[3]. The LPS-TLR4/MD2 complex activates downstream pro-inflammatory signaling pathways, including the transcription factor nuclear factor kappa-light-chain-enhancer of activated B cells (NF-κB) and mitogen-activated protein kinases (MAPKs), triggering the production of a variety of inflammatory cytokines. The excessive release of various pro-inflammatory cytokines result in the acute cellular and/or organic injury to form sepsis or ALI[4, 5]. Sepsis remains the leading cause of mortality in ICU[6] and leads to millions of deaths globally each year[7], and the outcomes of ALI also remain dismal with a morbidity and mortality rate around 40%[8].

So far, there is no specific and effective therapeutic strategy available to treat these acute inflammatory diseases. A novel and effective therapeutic agent is urgently required. A series of agents that target TLR4 have been investigated for the treatment of sepsis and ALI but have failed in pre-clinical study or in clinical trials[1]. In fact, although TLR4 is the central signaling receptor for LPS, LPS binds directly to the chaperone protein MD2, rather than directly to TLR4[9]. Recognition of LPS by TLR4 needs MD2. It has been demonstrated that MD2 is an essential protein for the intracellular distribution of TLR4 and recognition between TLR4 and LPS, and that MD2 knockout significantly reversed the LPS-induced endotoxic shock in mice[10]. Thus, increasing evidence has revealed that MD2 could be an important target for the discovery of anti-inflammatory agents.

The discovery of novel anti-inflammatory agents derived from natural active products has attracted a lot of attention from medicinal chemists. Cinnamic acid is a natural organic acid in plants with high safety and a variety of pharmacological activities, such as anti-oxidant, antimicrobial, anti-cancer, and anti-inflammatory activities[11, 12]. Due to their common occurence in plants and their low toxicity, cinnamic acid derivatives have been evaluated as

pharmacologically active compounds[13]. Among the derivatives, cinnamamide (Scheme 1) constitutes an interesting scaffold within medicinal chemistry thus it has been incorporated in several synthetic compounds with therapeutic potentials including neuroprotective, antimicrobial, anti-nociceptive, and anti-inflammatory properties[12, 14, 15]. We speculate that cinnamamide derivatives may represent beneficial pharmacological enhancements in anti-inflammatory action.

While a few derivatives of cinnamamides exhibited anti-inflammatory and/or analgesic activity, the current results of pharmacological evaluation did not lead to certain conclusions about the preferred type of substitution[15, 16]. The structure-activity relationship (SAR) among cinnamamides for their anti-inflammatory activity remains unclear. In addition, although previous studies performed the anti-inflammatory evaluation in LPS-stimulated cells or carrageenan-induced mouse paw edema[17], the possible mechanism and direct molecular targets by which cinnamanides exerted the anti-inflammatory effects were rarely investigated.

In the continuation of our study on the discovery of new anti-inflammatory agents from natural skeletons[18, 19], we proposed to find new cinnamanides with anti-inflammatory property for the treatment of acute inflammatory diseases, and to demonstrate the possible mechanism and molecular target. In this work, 34 cinnamamide derivatives were prepared and biologically evaluated (Scheme 1). Among these compounds, 2i showed the strongest anti-inflammatory activities *in vitro*. Furthermore, we identified the anti-inflammatory mechanism, molecular target, and *in vivo* pharmacology of 2i in mice with sepsis and ALI. Our results demonstrate that the new cinnamamide, 2i, is a novel MD2 inhibitor that exhibits the potential to treat sepsis and ALI.

Please insert Scheme 1

Results

Chemistry

Cinnamamide derivatives were prepared by the synthetic routes depicted in Scheme 1, and their structures are shown in Table 1. The intermediate products used in this method are the

appropriately substituted cinnamic acids (7w-7z). The cinnamic acids were either commercially available (7w) or were prepared from the corresponding substituted benzaldehydes (5x-5z) and malonic acid (6) via the Knoevenagel reaction. Target compounds were obtained through one-step amidation using substituted cinnamic acid and corresponding amines under the catalytic condition of EDC-HCl and HOBt. After stirred at 0–8°C for 1 h, the reaction mixture was maintained at room temperature for 4–8 h to generate a high yield of cinnamamides (Table 1), except for the dimer-type 1i-3i and 1k–3k. For 1i-3i and 1k-3k, two folds of substituted cinnamic acid were stirred with amines at 0-8°C for 20h. All of the compounds were identified by spectral analysis. By way of nuclear magnetic resonance spectra analysis (^{1}H NMR), the E configuration of the compounds was clearly demonstrated by the value of the vicinal coupling constant of the vinylic protons, which indicated a trans relationship between the two hydrogens. Pure compounds were obtained by either re-crystallization from $CHCl_3$/EtOH or by chromatography over silica gel column, and then HPLC with CH_3CN/CH_3OH as the solvent system was used to confirm the purity above 96.0%.

Please insert Table 1

Cinnamamides inhibited TNF-α and IL-6 production induced by LPS in macrophages

Thirty four synthesized cinnamamides were tested for their ability to inhibit LPS-induced release of tumor necrosis factor–α (TNF-α) in mouse primary peritoneal macrophages (MPMs). As shown in Figure 1A, while a majority of these compounds showed inhibition against LPS-induced TNF-α production to various degrees, only 4 compounds exhibited >50% inhibitory abilities compared to LPS alone group (1h, 2i, 3b and 3j). Based on the bio-screening results, we may observe some preliminary SAR conclusions. For example, (1) substitutions of the amide group with long-chain aliphatic substituents resulted in compounds with increased anti-inflammatory activity compare to the cyclic substituents; (2) in series 1, an electron-donating substitute in the amino moiety may decrease its inhibitory activity against TNF-α release, such as 1h, 1g and 1f; (3) in contrast, an electron-withdrawing halogen at the same site significantly increases the inhibitory effect; (4) in series 2, an electron-donating substitute in the amino moiety may increase the inhibitory activity against TNF-α secretion,

such as 2h, 2g and 2f; (5) a dimer structure with diamino group as a linker also maintained the anti-inflammatory properties. The quantitative SAR was also performed and described in the supporting information (Figure S1). We further tested the cytotoxicity of these compounds in MPMs. As shown in Figure S2, all cinnamamides showed no significant cytotoxicity in MPMs after 24h treatment. These four compounds were chosen for the next multi-dose evaluation in MPMs. As shown in Figure 1B and 1C, all of four compounds significantly suppressed the LPS-induced production of interleukin-6 (IL-6) and TNF-α. Especially, 3b at four concentrations inhibited TNF-α expression in a comparable degree. Although the response was barely dose-dependent, the multi-dose data validated the anti-inflammatory ability of these four compounds. Of these four, 2i exhibited the strongest inhibition against both TNF-α and IL-6 expression.

Please insert Figure 1

The active compound 2i prevented LPS-induced gene expression of pro-inflammatory cytokines and activation of MAPKs/NF-κB signaling pathways

Having excellent anti-inflammatory activity, 2i was further biologically evaluated (Figure 2A). We determined the inhibitory effect of 2i on the mRNA transcription of important pro-inflammatory proteins, including TNF-α, IL-1β, IL-6, COX-2, and PGES in LPS-stimulated macrophages. As shown in Figure 2B, real-time qPCR analysis revealed that 2i at 10 μM potently decreased the LPS-induced up-regulation of the mRNAs of these cytokines. In LPS-TLR4/MD2 pro-inflammatory signaling pathway, NF-κB and MAPKs (including p38, JNK, and ERK) have important roles in regulation of target cytokine gene expression. We investigated the possible involvement of NF-κB/MAPKs signaling in the anti-inflammatory action of 2i. While LPS elevated levels of p38, JNK, and ERK phosphorylation in MPMs, 2i pretreatment decreased LPS-induced phosphorylation of these three kinases in a dose-dependent manner (Figure 2C–E). NF-κB activation requires IκB degradation, causing NF-κB p65 submit translocation from the cytoplasm to the nucleus. We determined the effect of 2i on IκBα degradation and p65 nuclear translocation. The immunostaining data showed that LPS enhanced NF-κB p65 nuclear translocation (red point in blue nucleus), while in macrophages with 2i

pretreatment, nuclear p65 was dispersed and transferred outside the nuclei, suggesting that 2i inhibited p65 translocation (Figure 2F-H). In addition, we tested the inhibitory activity of 2i against NF-κB using a Luciferase Reporter system. As show in Figure S3, 2i could dose-dependently inhibit the transcriptional activity of NF-κB. Furthermore, LPS reduced IκBα levels and 2i pre-treatment reversed the degradation of IκBα in a dose-dependent manner (Figure 2I). Pretreatment of ERK or p38 inhibitor (PD98059 and SB239063, respectively) did not affect LPS-induced IκBα degradation, indicating that NF-κB and MAPKs signaling pathways are independent in LPS-TLR4/MD2 cascade (Figure 2I). These results indicate that the inhibition of MAPKs/NF-κB activation may mediate the anti-inflammatory effects of 2i.

Please insert Figure 2

Identification of MD2 as the molecular target of compound 2i

To identify the possible direct molecule target of 2i in LPS-TLR4/MD2 pathway (Figure S4), we investigated whether 2i could directly bind and inhibit the MAPKs and IKKβ, which is the kinase that regulates IκB activation and degradation. Recombinant kinases, including JNK2, ERK1, P38α, P38β, and IKKβ, were used to test the direct kinase-inhibitory activity of compound 2i in a cell-free system by Caliper Mobility Shift Assay. As shown in Table S1, 2i did not significantly inhibit any of these five kinases, indicating that an upstream target of MAPK/NF-κB might exist for the anti-inflammatory action of 2i.

TLR4 and MD2 are important proteins involved in LPS-induced inflammatory signaling. Upon binding to LPS, TLR4 proceeds to a physical receptor multimer consisting of two copies of the TLR4/MD2 complex. We next tested whether 2i directly targets TLR4 or MD2. The interaction between 2i and recombinant TLR4 or MD2 protein was determined by SPR experiments. As shown in Figure 3A and 3B, 2i did not interact with TLR4, but could dose-dependently bind to recombinant MD2 protein, with a KD value of 34 μM, suggesting that MD2 may be the direct target of 2i. We also tested the interaction of MD2 with 1f, a representative cinnamamide derivative without anti-inflammatory activity. The result in Figure S5 showed no interactions between MD2 and 1f. Hence, a series of biochemical experiments were designed and performed to validate this hypothesis. The fluorescent probe bis-ANS has

been used to test the lipid-binding sites of several proteins, including MD2[20, 21]. Figure 3C showed that fluorescence levels of bis-ANS were remarkably increased when binding to rhMD2 protein. However, co-incubation with 2i dose-dependently inhibited the intensity of bis-ANS fluorescence, indicating a displacement of bis-ANS by 2i from the rhMD2 pocket. Competition between 2i and LPS in binding to rhMD2 was detected by a biotin-streptavidin-based ELISA method. Figure 3D shows that biotin-LPS in the plates bound to rhMD2, while the co-incubation with 2i dose-dependently prevented the interaction between rhMD2 and biotin-LPS, suggesting that the binding sites for 2i on MD2 may overlap the binding sites for LPS. To demonstrate the effect of 2i on LPS binding to MD2 at the cellular level, macrophages were treated with FITC-labeled LPS (FITC-LPS) in the presence or absence of 2i and then proceeded to flow cytometric analysis. Pre-incubation with 2i significantly inhibited FITC-LPS binding to the cell surface (Figure 3E). In addition, an immunoprecipitation assay showed that 2i pretreatment potently inhibited LPS-induced formation of TLR4/MD2 complex in macrophages, indicating that 2i inhibited the interaction between TLR4 and secreted MD2 in macrophages (Figure 3F).

MD2 is a chaperone protein of TLR4 and is not associated with the activation of TLR2 pro-inflammatory signaling. Thus, a specific activator of TLR2, Pam3CK, was used to further investigate whether 2i specifically targets MD2 and inhibits the TLR4 signaling pathway. As shown in Figure 3G and 3H, compared to CU-CPT22, a specific TLR2 inhibitor, 2i failed to inhibit the production of IL-6 and TNF-α induced by the TLR2 agonist Pam3CK, indicating that 2i does not target TLR2 and the common downstream signaling of TLR2/TLR4. Taken together, these results are consistent with the observation that 2i binds directly to MD2 and antagonizes the formation of the LPS-TLR4/MD2 complex.

Please insert Figure 3

Study on 2i and MD2 binding sites

We then investigated the possible binding model and site of 2i binding to MD2. Since this is the first cinnamamide compound showing to target MD2 protein and no references could be used to speculate the binding mode, a computer-assistant structural simulation of the 2i-MD2 complex was firstly carried out as described in Method Section. The docking simulation showed

the binding model and sites of compound 2i with LPS/MD2/TLR4 complex and MD2 (Figure 4A). In consistent with the experimental data, the docking model reveals that 2i binds to the same hydrophobic pocket of MD2 to LPS, In the flexible binding simulation, two residues of MD2, Arg90, and Tyr 102, could form hydrogen bonds with the small-molecule ligand to stabilize the binding conformation. These two residues showed no interaction with the structure of LPS buried in the MD2 pocket. Thus, the next step is to confirm the roles of Tyr102 and Arg90 in 2i binding to MD2. Two recombinant mutants, $MD2^{R90A}$ and $MD2^{Y102A}$, were constructed and used in further assays. As shown in Figure S6A-C, either R90A or Y102A mutation did not affect the LPS-rhMD2 interaction. However, Figure 4B shows that 2i failed to inhibit the binding between Biotin-LPS and $MD2^{R90A}$. SPR assay revealed that the ability of 2i to directly bind $MD2^{R90A}$ was abolished (Figure 4C). Similar results were observed when Tyr102 was mutated to Ala (Figure 4D and 4E). These results suggest the possible binding mechanism and sites for 2i with MD2 protein.

Please insert Figure 4

Effect of 2i administration on the survival rate of LPS-induced septic mice

To determine whether 2i was able to attenuate the development of endotoxic shock by inhibiting the LPS-induced inflammatory response, LPS at 20mg/kg was intraperitoneally (i.p.) injected into the mice with or without 2i pre-treatment. The mice were then monitored for 7 days. As shown in Figure 5, all mice in the LPS alone group died within 48 h as a result of sepsis. Conversely, 100% of the animals that received 2i at 10 mg/kg before LPS injection survived. Thus, 2i showed excellent anti-inflammatory activity *in vivo*.

Please insert Figure 5

Compound 2i attenuated LPS-induced acute lung injury in mice

ALI was induced in mice by intratracheal LPS instillation to further evaluate the protective ability of 2i against LPS-induced acute inflammation *in vivo*. As shown in Figure 6A, a marked increase in the protein concentration in mice BALF was observed after LPS instillation and the

increase was significantly inhibited by 2i treatment. The lung wet/dry weight ratio, which is an index of lung edema, was significantly increased in the LPS alone group when compared to both the control saline group and the LPS + 2i group, indicating that 2i also suppressed LPS-induced lung edema (Figure 6B). Recruitment of neutrophils into the pulmonary compartment is an important feature of ALI. As shown in Figure 6C and 6D, LPS challenge caused a strong increase in the number of neutrophils and total cells in the bronchial alveolar lavage fluid (BALF), while treatment with 2i significantly decreased the numbers of both neutrophils and total cells in BALF from ALI mice. MPO activity in tissues is an indicator of neutrophil infiltration. Figure 6E shows that treatment with 2i significantly decreased LPS-induced MPO activity in mice lung tissues. To evaluate the histological changes, mice lung tissues were proceeded to hematoxylin and eosin (H&E) staining (Figure 6F). Mice in the control group exhibited a normal structure of lung tissues under a light microscope, while LPS instillation resulted in significant pulmonary congestion, infiltration of inflammatory cells, thickening of the alveolar wall, and interstitial edema. These pathological changes induced by LPS were remarkably reduced by 2i treatment. Figure 6G further validated the inhibitory effect of 2i against macrophage infiltration into the lung, as evidenced by the reduced CD68 expression in LPS + 2i group.

LPS exposure also increased the mRNA expression of inflammatory cytokines such as IL-6, TNF-α, and IL-1β in mice lung tissues, which were all significantly reduced by 2i treatment (Figure 6H-6J). We also observed the anti-inflammatory effect of 2i in cultured human lung cells. As shown in Figure S7, pre-treatment with 2i reduced the LPS-induced transcription of IL-6, TNF-α, IL-1β, and COX-2 in the human lung epithelial Beas-2B cells. Finally, we investigated whether the pharmacological activity of 2i was associated with its inhibition of MD2 and subsequent TLR4/MD2 complex formation. As shown in Figure 6K, compared with the control group, LPS treatment significantly induced the formation of the TLR4/MD2 complex in mouse lung tissues, while 2i administration reduced the level of TLR4/MD2 complex. These data indicate that the MD2 inhibitor 2i exerts an anti-inflammatory and anti-ALI activity in LPS-induced mice lungs.

Please insert Figure 6

Discussion and conclusions

Acute inflammatory diseases remain the main cause of death in intensive care units worldwide and still lack of effective therapy in the clinical treatment. Steroidal and non-steroidal anti-inflammatory drugs have been found to be therapeutically limited in the treatment of sepsis and ALI[22, 23]. Cinnamamide is a unique template, which has been reported to possess a variety of biological activities, including anti-inflammatory and anti-cancer activities[11, 15, 24]. The safety and convenience of preparation also contribute to the feasibility of developing bioactive molecules from cinnamamide-based compounds[25]. In this study, we present a series of novel cinnamamides with potent anti-inflammatory activities both *in vitro* and *in vivo*, and more importantly, that we demonstrat the biological mechanism and target for the anti-inflammatory action of dimer-type cinnamamide 2i.

Although there are several examples in the literature of the anti-inflammatory activity of cinnamamide derivatives[15], the structure-activity relationship (SAR) remains limited. Here, anti-inflammatory effects of 34 cinnamamide-structural MACs were evaluated in LPS-stimulated macrophages and the preliminary SAR conclusions were obtained. In addition, we also performed a quantitative SAR analysis as described in the Supporting Information. The relationship between the anti-inflammatory activity and Some structural descriptors of compounds were found to be able to relate with the anti-inflammatory activity. Shown in Figure S1 is the scatter plot for experimental and computational value of each compound, with a highly squared regression coefficient ($R^2_{adj} = 0.71$), which can describe more than 71% of the variance observed in the experimental activity. The QSAR result indicates that the size and shape of molecules, as well as their steric properties, play important roles in the SAR of cinnamamides.

Among these synthetic cinnamamides, a compound contain a dimer motif, 2i, was identified as the most active compound. 2i was able to significantly inhibit the mRNA expression of inflammatory cytokines, NF-κB activation, and MAPKs phosphorylation in LPS-stimulated macrophages. In addition, we tested the pharmacokinetic (PK) profiles of compound 2i in rats (Figure S10A-C). With 20 mg/kg oral administration, the peak concentration of 2i reached 0.27μg/ml and decreased to 0.04 ug/ml after 12h (Figure S10B);

with 10mg/kg intravenous administration, the peak concentration of 2i reached 0.55ug/ml and decreased to 0.04ug/ml after 24h (Figure S10C). These data imply that 2i could be potentially developed as a novel anti-inflammatory agent for the treatment of acute inflammatory diseases.

Thus, it is important to investigate and identify the possible molecular target of 2i. For small-molecule drugs, which comprise most of the medicines available today, the identification of the molecular targets underlying the therapeutic effect of the drug and/or their adverse side effects remains a key challenge[26, 27]. After finding the inhibition of 2i on cytokine proteins and mRNAs, we employed a backstepping method to find the molecular target of 2i in LPS-TLR4/MD2 pro-inflammatory cascade. MAPKs and NF-κB are important signaling components in the LPS-TLR4/MD2 pro-inflammatory pathway, which is activated upon LPS stimulation in a MyD88-dependent manner, and subsequently trigger the transcription of pro-inflammatory genes. Although our data in Figure 2 showed the ability of 2i in inhibiting the activation of MAPKs and NF-κB, Table S1 showed that 2i failed to directly inhibit the activity of these recombinant kinases, suggesting that 2i may act on the upstream target in the LPS-TLR4/MD2 pathway. We then tested the direct interaction between 2i and TLR4 or MD2, respectively, and found that 2i could bind to a recombinant MD2 protein with a KD value of 34 μM. Subsequently, some experiments at both molecular and cellular levels were designed to further confirm this finding. Fluorescence measurements validated the direct binding of 2i to rhMD2 protein, and ELISA confirmed the effect of 2i on the binding of LPS and rhMD2. Immunoprecipitation and flow cytometry showed that 2i affected LPS-MD2 interactions and the formation of MD2-TLR4 complex. In addition, our results in Figure 3F and 6K showed that, without LPS stimulation, TLR4 and MD2 can bind to each other in a low degree, while LPS stimulation promote the formation of a lot of TLR4/MD2 complex. Thus, we presume that LPS induces the formation of TLR4 and MD2 and 2i inhibits the formation of TLR4 and MD2 complex in macrophages. However, other group found that TLR4 and MD2 could form complex in Golgi apparatus without LPS stimulation in embryonic fibroblasts[10]. We may consider that 2i inhibits the interaction between TLR4 and secreted MD2 in macrophages and that there may exist cell-type difference in the TLR4/MD2 signaling regulation. We also found that 2i showed no inhibitory effect against TLR2-mediated cytokine expression which is independent of MD2 activity. Taken together, these data clearly show that 2i is a novel inhibitor of MD2.

Recently, a few natural and synthetic molecules have been found to target and inhibit MD2 protein and then to prevent LPS-induced inflammatory responses[28-30]. This is the first time to find cinnamamide could binds MD2 protein, while some small molecules, which contain the cinnamaldehyde skeleton and α,β-unsaturated carbonyl moiety in structure, were found to bind MD-2. So far, more than seven cinnamaldehyde skeleton-containing MD-2 inhibitors were identified, including JSH[29], CAPE[31], curcumin[28], xanthohumol[30], 1D10G[32], and two compounds L6H21 and L48H37 found by our group[33, 34]. Their chemical structures are shown in Figure S8. They directly interact MD-2 pocket, inhibiting the activation of LPS-MD2/TLR4 signaling and preventing LPS-induced inflammatory response and septic shock. These inhibitors share similar chemical structure, cinnamaldehyde moiety, with cinnamamides. This note also strengthens our confidence on the fact that cinnamamide 2i directly binds MD2 and inhibits MD2-LPS interaction. In addition, we also compared 2i with two previously reported natural MD2 inhibitors, curcumin[35] and xanthohumol (Figure S9), two compounds with the cinnamaldehyde structure. The KD values of 2i-MD2, xanthohumol-MD2, and curcumin-MD2 are 0.000034M, 0.00046M[35], and 0.000379M, respectively. Our results showed 2i has a stronger interaction than curcumin and xanthohumol towards rhMD2 protein.

Until now, no crystal structure of the complex of small-molecule inhibitor and MD2 protein has been reported. The previous X-ray diffraction-based structural characterization showed that a β cup fold and two antiparallel β sheets, form a hydrophobic pocket in mature MD2 containing 143 amino acid residues[36, 37]. The MD2 pocket is deep and narrow, with a volume of about 1700 $Å^3$. The hydrophobic residues are coated on the internal surface of the pocket, and some residues with positive charges are located near the opening rim of the cavity[36, 37]. In the flexible binding simulation, 20 conformations of 2i formed two hydrogen bonds with Arg90 and Tyr102 residues of MD2, indicating their importance in the molecular interaction. Then, two mutated forms of MD2, $MD2^{R90A}$ and $MD2^{Y102A}$, were employed to validate this finding. Previously, some residues Lys122, Tyr102, Gly123, Ser120, Lys130, and Phe126 in the MD2 protein pocket have been predicted as key binding sites in the interactions between MD2 and non-lipid inhibitors such as JSH[29], taxanes[38], and xanthohumol[30]. In addition, Cys133 was considered to form covalent bonds via a Michael-type reaction when CAPE binds MD2[31]. However, it seems to be of no role in the interaction between MD2 and curcumin[28], despite that both CAPE and

curcumin have the α,β-unsaturated carbonyl moiety. Our previous studies revealed the importance of Arg90 and Tyr102 residues in the binding of L6H21 and L48H37 with MD2[33, 34]. This study demonstrates that Arg90 and Tyr102 are also important residues involved in the 2i-MD2 interaction.

Both pharmacological and genetic MD2 inhibition has been reported to inhibit LPS-induced inflammatory responses and the development of sepsis. Acute inflammatory diseases such as sepsis induced by endotoxin have received increased awareness due to their prevalence and poor therapy options. Therapies through neutralizing both inflammatory cytokine TNF-α and signaling proteins CD14 and TLR4 already failed in clinical trials[39]. Therefore, to validate the clinical efficacy of agents targeting MD2 is very important. A lipid-like TLR4/MD2 antagonist eritoran was evaluated in clinical study for the treatment of sepsis. However, the Phase III clinical study showed that eritoran failed to cure severe sepsis[1]. Also, none of small-molecule inhibitors of MD2 have been pursued in clinical trials. Our study found that the MD2 inhibitor 2i could prevent LPS-induced septic shock at an unbelievable 100% level, indicating that 2i may be a potential candidate for sepsis therapy.

More importantly, we demonstrate for the first time, that MD2 inhibition could significantly attenuate ALI in animal models. ALI is a critical illness that is characterized by noncardiogenic edema, pulmonary inflammation, severe systemic hypoxemia, decreased neutrophil apoptosis in the lung, and multiple organ failure[40]. Numerous pharmacological therapies for established ALI, including corticosteroids and steroids, have failed to show benefit in multicenter clinical trials[41]. Thus, new agents are still urgently needed for ALI therapy. Since LPS is a common cause of ALI, the TLR4/MD2 receptor complex could be considered as a therapeutic target of ALI. Hadina et al. showed that MD2-null mice do not respond to nasal aspiration of LPS from Neisseria meningitides[42]. 2i significantly attenuated LPS-induced lung injury as well pulmonary inflammation, accompanied with reduced MD2/TLR4 complex formation in lung tissue. These results show that 2i inhibited the development of LPS-induced ALI by targeting MD2 and inhibiting the MD2/TLR4-dependent inflammatory responses in mouse lung (Figure 7). Therefore, it is also suggested that MD2 inhibition is a potential therapeutic strategy for ALI in the future.

Please insert Figure 7

In conclusion, 34 cinnamamide derivatives were synthesized, their bioactivities were evaluated against LPS-induced inflammation. The most active compound 2i, which contain a dimer motif, was further investigated for the molecular target and anti-inflammation activity both *in vitro* and *in vivo*. Our data shows that 2i significantly blocked LPS-induced pro-inflammatory gene expression and MAPKs/NF-κB activation *in vitro* and prevented LPS-caused septic shock and ALI *in vivo*. Mechanistically, these anti-inflammatory actions of 2i seem to be mediated by directly targeting and inhibiting MD2. Arg90 and Tyr102 in the MD2 protein are key residues in the interaction between 2i and MD2 protein. Taken together, this study presents a new MD2 inhibitor, 2i, which deserves further development as a potential candidate for the therapy of sepsis and ALI, and more importantly, this work finds the first cinnamamide-structural MD2 inhibitor and suggests a new lead structure for the development of anti-inflammatory agents targeting MD2.

Experimental Section

Reagents

Chemical reagents, ERK inhibitor PD98059, p38 inhibitor SB239063, and LPS were purchased from Sigma (Louis, MO). Recombinant human TLR4 (rhTLR4) protein and TLR2 inhibitor CU-CPT22 were purchased from R&D Systems, Inc. (Minneapolis, MN, USA). Recombinant human MD2 (rhMD2) and mutated rhMD2 was obtained using the methods described in our previous publication[34].

Chemical synthesis

Melting points were determined on a Fisher-Johns melting apparatus and were uncorrected. ^{1}H NMR spectra were recorded on a Bruker AVANCE III 600 spectrometer. The chemical shifts were presented in terms of parts per million with TMS as the internal reference. Electron-spray ionization mass spectra in positive mode (LC-ESI-MS) data were recorded on a Bruker Esquire HCT spectrometer. Column chromatography purifications were carried out on Silica Gel 60 (E.

Merck, 70–230 mesh). The purity of all target compounds was confirmed to be greater than 96% by HPLC analysis conducted on an Agilent 1260 liquid chromatograph system. The chromatography was carried out at room temperature using a ZORBAX SB-C18 column (150 × 4.6 mm, 5 μm) and a gradient of 10−90% acetonitrile in methanol in 20 min. The detection wavelength was set at 254 nm.

The general procedure for synthesis of cinnamamides was two steps including knoevenagel reaction and amidation. Briefly, an amount of 20 mmol different substituted arylaldehyde and 24 mmol malonic acid were mixed with 0.5mmol amidobenzene to give corresponding cinnamic acid. The mixture was stirred at 95 ^{o}C and monitored with TLC ($CH_3COOEt/CHCl_3$). When the reaction was finished, 3mol/L HCl was dropped into the residue until no new solid was precipitated. The precipitate was filtered and washed with water and cold ethanol, and dried in vacuum. The intermediate was purified after recrystallization. The target compounds were prepared by condensation of the corresponding cinnamic acids with various amines utilizing 1-(3-dimethylamino-propyl)-3-ethylcarbodiimide hydrochloride (EDC) and 1-hydroxybenzotriazole (HOBT) as catalyst in methylene chloride. An amount of 1.65mmol EDC·HCl and 1.95mmol HOBt was stirred with the 1.50 mmol cinnamic acid at 0-8 ^{o}C. After 10 min, the 1.50 mmol amine was added,and the mixture was stirred at 0-8 ^{o}C for 1h before room temperature reaction (for dimer-type series 1i-3i and 1k-3k, 0.75 mmol amine was added and stirred at 0-8°C for 20h). The procedure was monitored with TLC until the reaction was finished. The residue was washed with saturated $NaHCO_3$ solution and extracted with CH_2Cl_2. After solvent evaporation, the solid was purified by chromatography over silica gel to yield compounds. Their structures were characterized by spectral data from MS and 1H NMR. The spectral data of novel or unreported compounds are listed as the following.

(E)-3-(2,3-Dichlorophenyl)-1-morpholinoprop-2-en-1-one(1a): Yellow powder, 85.3% yield, mp 125.3-127.1°C. ^{1}H-NMR ($CDCl_3$): δ (ppm) 3.74 (8H, br.s,-CH_2-×4), 6.79 (1H, d, J = 15.0 Hz, =CH-C=O), 7.19-7.25 (1H, m, Ar-H^{6}), 7.43-7.48 (1H, m, Ar-H^{5}), 7.43-7.48 (1H, m, Ar-H^{4}), 8.01 (1H, d, J = 15.0 Hz, Ar-CH=C). ESI-MS *m/z*: 286.2$(M)^{+}$, 308.0 $(M+Na-1)^{+}$, calcd for $C_{13}H_{13}Cl_2NO_2$: 286.15.

(E)-N-butyl-3-(2,3-Dichlorophenyl)acrylamide(1b): Yellow powder, 83.2% yield, mp 107.0-108.8°C. ^{1}H-NMR ($CDCl_3$): δ (ppm) 0.94 (3H, t, J = 7.2 Hz, C-CH_3), 1.35-1.42 (2H, m, -CH_2-C), 1.53-1.58 (2H, m, -CH_2-C-C), 3.37-3.41 (2H, m, N-CH_2-), 6.37 (1H, d, J = 15.6 Hz, =CH-C=O), 7.16-7.19 (1H, m, Ar-H^6), 7.42-7.44 (1H, m, Ar-H^5) ,7.42-7.44 (1H, m, Ar-H^4), 7.95 (1H, d, J = 15.6 Hz, Ar-CH=C). ESI-MS *m/z*: 272.1 $(M)^+$, 294.0 $(M+Na-1)^+$, calcd for $C_{13}H_{15}Cl_2NO$: 272.17.

(E)-N-Benzyl-3-(2,3-dichlorophenyl)acrylamide(1c): Yellow powder, 79.6% yield, mp 175.7-177.1°C. ^{1}H-NMR ($CDCl_3$): δ (ppm) 4.58 (2H, d, J = 5.4 Hz, Ar-CH_2), 6.40 (1H, d, J = 15.6 Hz, =CH-C=O), 7.17-7.20 (1H, m, Ar-H^6), 7.26-7.36 (5H, m, Ar-H×5), 7.44-7.45 (1H, m, Ar-H^5), 7.44-7.45 (1H, m, Ar-H^4) , 7.99(1H, d, J = 15.6 Hz, Ar-CH=C). ESI-MS *m/z*: 306.6 $(M)^+$, 308.4$(M+2)^+$, calcd for $C_{16}H_{13}Cl_2NO$: 306.19.

(E)-3-(2,3-Dichlorophenyl)-N-phenethylacrylamide(1d): Yellow powder, 82.1% yield, mp 151.3-153.0°C. ^{1}H-NMR ($CDCl_3$): δ (ppm) 2.90 (2H, t, J = 6.6 Hz, Ar-CH_2), 3.65-3.69 (2H, m, Ar-C-CH_2-.), 6.30 (1H, d, J = 15.6 Hz, =CH-C=O), 7.16-7.19 (1H, m, Ar-H^6), 7.25-7.43 (5H, m, Ar-H×5), 7.43-7.44 (1H, m, Ar-H^5), 7.43-7.44 (1H, m, Ar-H^4) , 7.94 (1H, d, J = 15.6 Hz, Ar-CH=C). ESI-MS *m/z*: 320.2 $(M)^+$, 322.1 $(M+2)^+$, calcd for $C_{17}H_{15}Cl_2NO$: 320.21.

(E)-3-(2,3-Dichlorophenyl)-N-(3-phenylpropyl)acrylamide(1e): Yellow powder, 79.6% yield, mp 89.6-91.1°C. ^{1}H-NMR ($CDCl_3$): δ (ppm) 1.88-1.92 (2H, m, Ar-C-CH_2-), 2.68 (2H, t, J = 7.2 Hz, Ar-CH_2-), 3.40-3.43 (2H, m, Ar-C-C-CH_2-), 6.38 (1H, d, J = 15.6 Hz, =CH-C=O), 7.13-7.15 (1H, m, Ar-H^6), 7.15-7.28 (5H, m, Ar-H×5), 7.40-7.42 (1H, m, Ar-H^5), 7.40-7.42 (1H, m, Ar-H^4) , 7.93 (1H, d, J = 15.6 Hz, Ar-CH=C). ESI-MS *m/z*: 334.2 $(M)^+$, 356.1 $(M+Na-1)^+$, calcd for $C_{18}H_{17}Cl_2NO$: 334.24.

(E)-3-(2,3-Dichlorophenyl)-N-(3,4-dimethoxybenzyl)acrylamide(1f): Yellow powder, 83.5% yield, mp 169.4-170.5°C. ^{1}H-NMR ($CDCl_3$): δ (ppm) 3.89 (3H, s, Ar-OCH_3^4), 3.90 (3H, s, Ar-OCH_3^3), 4.54 (2H, d, J = 5.4 Hz, Ar-CH_2), 6.41 (1H, d, J = 15.6 Hz, =CH-C=O), 6.85 (1H, d, J = 8.4 Hz, Ar^2-H^5), 6.90 (1H, d, J = 8.4 Hz, Ar^2-H^6), 6.91 (1H, s, Ar^2-H^2), 7.20-7.22 (1H, m,

Ar-H^6), 7.46-7.48 (1H, m, Ar-H^5), 7.46-7.48 (1H, m, Ar-H^4), 8.03 (1H, d, *J* = 15.6 Hz, Ar-CH=C).ESI-MS *m/z*: 366.1 $(M)^+$, 388.0 $(M+Na-1)^+$, calcd for $C_{18}H_{17}Cl_2NO_3$: 366.24.

(E)-3-(2,3-Dichlorophenyl)-N-(4-methoxyphenethyl)acrylamide(1g): Yellow powder, 79.6% yield, mp 159.0-160.5°C. ^{1}H-NMR ($CDCl_3$): δ (ppm) 2.83 (2H, t, *J* = 6.6 Hz, Ar-CH_2), 3.61-3.64 (2H, m, Ar-C-CH_2-.), 3.79 (3H, s, Ar-OCH_3), 6.30 (1H, d, *J* = 15.6 Hz, =CH-C=O), 6.86 (2H, d, *J* = 9.0 Hz, Ar^2-H^{3,5}), 7.14 (2H, d, *J* = 9.0 Hz, Ar^2-H^{2,6}), 7.17-7.19 (1H, m, Ar-H^6), 7.42-7.44 (1H, m, Ar-H^5), 7.42-7.44 (1H, m, Ar-H^4),7.95(1H, d, *J* = 15.6 Hz, Ar-CH=C). ESI-MS *m/z*: 350.2 $(M)^+$, 372.1 $(M+Na-1)^+$, calcd for $C_{18}H_{17}Cl_2NO_2$: 350.24.

(E)-3-(2,3-Dichlorophenyl)-N-(4-fluorobenzyl)acrylamide(1h): Yellow powder, 73.3% yield, mp 169.5-171.3°C. ^{1}H-NMR ($CDCl_3$): δ (ppm) 4.57 (2H, d, *J* = 6.0 Hz, Ar-CH_2-), 6.41 (1H, d, *J* = 15.6 Hz, =CH-C=O), 7.04-7.07 (2H, m, Ar^2-H^{3,5}), 7.20-7.22 (1H, m, Ar-H^6), 7.32-7.34 (2H, m, Ar^2-H^{2,6}), 7.45-7.48 (1H, m, Ar-H^5), 7.45-7.48 (1H, m, Ar-H^4), 8.04(1H, d, *J* = 15.6 Hz, Ar-CH=C). ESI-MS *m/z*: 324.2 $(M)^+$, 346.1 $(M+Na-1)^+$, calcd for $C_{16}H_{12}Cl_2FNO$: 324.18.

(2E,2'E)-N,N'-(Ethane-1,2-diyl)bis(3-(2,3-dichlorophenyl)acrylamide)(1i): Yellow powder, 54.3% yield, mp 239.8-241.4°C. ^{1}H-NMR (DMSO): δ (ppm) 3.16 (4H, s, -CH_2-×2), 6.68 (2H, d, *J* = 15.6 Hz, =CH-C=O×2), 7.41-7.43 (2H, m, Ar-H^6×2), 7.66-7.67(2H, m, Ar-H^5×2), 7.66-7.67(2H, m, Ar-H^4×2) , 7.74 (2H, d, *J* = 15.6 Hz, Ar-CH=C×2), 8.46(2H, s, -NH-×2). ESI-MS *m/z*: 458.9 $(M+1)^+$, calcd for $C_{20}H_{16}Cl_4N_2O_2$: 458.17.

(E)-N-(4-Chlorobenzyl)-3-(2,3-dichlorophenyl)acrylamide(1j): Yellow powder, 76.2% yield, mp 205.7-207.5°C. ^{1}H-NMR (DMSO): δ (ppm) 4.38 (2H, d, *J* = 5.4 Hz, Ar-CH_2), 6.73 (1H, d, *J* = 15.6 Hz, =CH-C=O), 7.31 (2H, d, *J* = 8.4 Hz, Ar^2-H^{2,6}), 7.39 (2H, d, *J* = 8.4 Hz, Ar^2-H^{3,5}),7.40-7.42 (1H, m, Ar-H^6), 7.65-7.67 (1H, m, Ar-H^5), 7.65-7.67 (1H, m, Ar-H^4), 7.75(1H, d, *J* = 15.6 Hz, Ar-CH=C), 8.80 (1H, s, -NH-). ESI-MS *m/z*: 340.0 $(M)^+$,calcd for $C_{16}H_{12}Cl_3NO$: 340.63.

(2E,2'E)-N,N'-(Hexane-1,6-diyl)bis(3-(2,3-dichlorophenyl)acrylamide)(1k): Yellow powder, 44.5% yield, mp 199.3-201.1°C. ^{1}H-NMR (DMSO): δ (ppm) 1.30 (4H, m, -N-C-C-CH_2×2), 1.45(4H, m, -N-C-CH_2×2), 3.17(4H, m, -N-CH_2×2), 6.67 (2H, d, *J* = 15.6 Hz, =CH-C=O×2), 7.38-7.41 (2H, m, Ar-H^6×2), 7.63-7.64 (2H, m, Ar-H^5×2), 7.63-7.64(2H, m, Ar-H^4×2) , 7.68 (2H, d, *J* = 15.6 Hz, Ar-CH=C×2), 8.24(2H, t, *J* = 5.4 Hz, -NH-×2). ESI-MS *m/z*: 514.9 $(M+1)^+$, calcd for $C_{24}H_{24}Cl_4N_2O_2$: 514.27.

(E)-3-(2,4-Dimethoxyphenyl)-1-morpholinoprop-2-en-1-one(2a): Yellow powder, 84.3% yield, mp 60.6-62.3°C. ^{1}H-NMR ($CDCl_3$): δ (ppm) 3.71 (8H, br.s, -CH_2-×4), 3.82 (3H, s, Ar-OCH_3^4), 3.85 (3H, s, Ar-OCH_3^2), 6.44 (1H, s, Ar-H^3), 6.48 (1H, d, *J* = 8.4 Hz, Ar-H^5), 6.86 (1H, d, *J* = 15.6 Hz, =CH-C=O), 7.40 (1H, d, *J* = 8.4 Hz, Ar-H^6), 7.85 (1H, d, *J* = 15.6 Hz, Ar-CH=C). ESI-MS *m/z*: 278.1 $(M+1)^+$, 300.1 $(M+Na)^+$, calcd for $C_{15}H_{19}NO_4$: 277.32.

(E)-N-Butyl-3-(2,4-dimethoxyphenyl)acrylamide(2b): Yellow powder, 76.4% yield, mp 99.0-100.8°C. ^{1}H-NMR ($CDCl_3$): δ (ppm) 0.94 (3H, t, *J* = 7.2 Hz, C-CH_3), 1.35-1.39 (2H, m, -CH_2-C), 1.51-1.54 (2H, m, -CH_2-C-C), 3.35-3.38 (2H, m, N-CH_2-), 3.82 (3H, s, Ar-OCH_3^4), 3.84 (3H, s, Ar-OCH_3^2), 6.41 (1H, s, Ar-H^3), 6.45 (1H, d, *J* = 8.4 Hz, Ar-H^5), 6.47 (1H, d, *J* = 15.6 Hz, =CH-C=O), 7.37 (1H, d, *J* = 8.4 Hz, Ar-H^6), 7.76 (1H, d, *J* = 15.6 Hz, Ar-CH=C). ESI-MS *m/z*: 264.0 $(M+1)^+$, 286.0 $(M+Na)^+$, calcd for $C_{15}H_{21}NO_3$: 263.33.

(E)-3-(2,4-Dimethoxyphenyl)-N-phenethylacrylamide(2d): Yellow powder, 81.1% yield, mp 102.3-103.8°C. ^{1}H-NMR ($CDCl_3$): δ (ppm) 2.87 (2H, t, *J* = 7.2 Hz, Ar-CH_2-), 3.64 (2H, m, Ar-C- CH_2-), 3.81 (3H, s, Ar-OCH_3^4), 3.82 (3H, s, Ar-OCH_3^2), 6.38 (1H, d, *J* = 15.6 Hz, =CH-C=O), 6.43(1H, s, Ar-H^3), 6.45 (1H, d, *J* = 8.4 Hz, Ar-H^5), 7.21-7.32 (5H, m, Ar-H×5), 7.37 (1H, d, *J* = 8.4 Hz, Ar-H^6) , 7.78 (1H, d, *J* = 15.6 Hz, Ar-CH=C). ESI-MS *m/z*: 312.1$(M+1)^+$, 334.0 $(M+Na)^+$, calcd for $C_{19}H_{21}NO_3$: 311.37.

(E)-3-(2,4-Dimethoxyphenyl)-N-(3-phenylpropyl)acrylamide(2e): Yellow powder, 75.1% yield, mp 69.5-71.2°C. ^{1}H-NMR ($CDCl_3$): δ (ppm) 1.86-1.91 (2H, m, Ar-C-CH_2-), 2.68 (2H, t, *J* = 7.2 Hz, Ar-CH_2-), 3.39-3.42 (2H, m, Ar-C-C-CH_2-), 3.81 (3H, s, Ar-OCH_3^4), 3.83 (3H, s,

Ar-OCH_3^2), 6.40 (1H, d, *J* = 15.6 Hz, =CH-C=O), 6.43 (1H, s, Ar-H^3), 6.45 (1H, d, *J* = 8.4 Hz, Ar-H^5), 7.16-7.28 (5H, m, Ar-H×5), 7.37 (1H, d, *J* = 8.4 Hz, Ar-H^6) , 7.76 (1H, d, *J* = 15.6 Hz, Ar-CH=C). ESI-MS *m/z*: 326.1 $(M+1)^+$, 348.0 $(M+Na)^+$, calcd for $C_{20}H_{23}NO_3$: 325.40.

(E)-N-(3,4-Dimethoxybenzyl)-3-(2,4-dimethoxyphenyl)acrylamide(2f): Yellow powder, 70.1% yield, mp 159.0-160.8°C. ^{1}H-NMR ($CDCl_3$): δ (ppm) 3.82 (3H, s, Ar-OCH_3^4), 3.84 (3H, s, Ar-OCH_3^2), 3.86 (3H, s, Ar^2-OCH_3^4), 3.88 (3H, s, Ar^2-OCH_3^3), 4.49(1H, d, *J* = 5.4 Hz, Ar-CH_2), 6.44 (1H, d, *J* = 15.6 Hz, =CH-C=O), 6.45(1H, s, Ar-H^3), 6.47 (1H, d, *J* = 8.4 Hz, Ar-H^5), 6.81 (1H, d, *J* = 8.4 Hz, Ar^2-H^5), 6.86 (1H, d, *J* = 8.4 Hz, Ar^2-H^6), 6.88 (1H, s, Ar^2-H^2), 7.38 (1H, d, *J* = 8.4 Hz, Ar-H^6) , 7.80 (1H, d, *J* = 15.6 Hz, Ar-CH=C). ESI-MS *m/z*: 358.1 $(M+1)^+$, 380.0 $(M+Na)^+$, calcd for $C_{20}H_{23}NO_5$: 357.40.

(E)-3-(2,4-Dimethoxyphenyl)-N-(4-methoxyphenethyl)acrylamide(2g): Yellow powder, 69.5% yield, mp 121.5-123.0°C. ^{1}H-NMR ($CDCl_3$): δ (ppm) 2.81 (2H, t, *J* = 6.6 Hz, Ar-CH_2), 3.58-3.61 (2H, m, Ar-C-CH_2-), 3.79 (3H, s, Ar^2-OCH_3), 3.81 (3H, s, Ar-OCH_3^4), 3.83 (3H, s, Ar-OCH_3^2), 6.35 (1H, d, *J* = 15.6 Hz, =CH-C=O), 6.43 (1H, s, Ar-H^3), 6.46 (1H, d, *J* = 8.4 Hz, Ar-H^5), 6.85 (2H, d, *J* = 8.4 Hz, Ar^2-$H^{3,5}$), 7.13 (2H, d, *J* = 8.4 Hz, Ar^2-$H^{2,6}$), 7.37 (1H, d, *J* = 8.4 Hz, Ar-H^6), 7.76 (1H, d, *J* = 15.6 Hz, Ar-CH=C). ESI-MS *m/z*: 342.1 $(M+1)^+$, 364.0 $(M+Na)^+$, calcd for $C_{20}H_{23}NO_4$: 341.40.

(E)-3-(2,4-Dimethoxyphenyl)-N-(4-fluorobenzyl)acrylamide(2h): Yellow powder, 80.1% yield, mp 152.2-154.1°C. ^{1}H-NMR ($CDCl_3$): δ (ppm) 3.82 (3H, s, Ar-OCH_3^4), 3.84 (3H, s, Ar-OCH_3^2), 4.52 (2H, d, *J* = 6.0 Hz, Ar-CH_2), 6.44 (1H, d, *J* = 15.6 Hz, =CH-C=O), 6.47 (1H, s, Ar-H^3), 6.48 (1H, d, *J* = 8.4 Hz, Ar-H^5), 6.99-7.02 (2H, m, Ar^2-$H^{3,5}$), 7.28-7.30 (2H, m, Ar^2-$H^{2,6}$), 7.38 (1H, d, *J* = 8.4 Hz, Ar-H^6), 7.80 (1H, d, *J* = 15.6 Hz, Ar-CH=C). ESI-MS *m/z*: 316.1 $(M+1)^+$, 338.0 $(M+Na)^+$, calcd for $C_{18}H_{18}FNO_3$: 315.34.

(2E,2'E)-N,N'-(Ethane-1,2-diyl)bis(3-(2,4-dimethoxyphenyl)acrylamide)(2i): Yellow powder, 35.6% yield, mp 194.2-194.8°C. ^{1}H-NMR (DMSO): δ (ppm) 3.74 (4H, s, -CH_2×2), 3.78 (6H, s, Ar-OCH_3^4×2), 3.84 (6H, s, Ar-OCH_3^2×2), 6.50 (2H, d, *J* = 15.6 Hz, =CH-C=O×2),

6.57 (2H, d, J = 8.4 Hz, Ar-H^5×2), 6.60 (2H, s, Ar-H^3×2), 7.44 (2H, d, J = 8.4 Hz, Ar-H^6×2) , 7.58 (2H, d, J = 15.6 Hz, Ar-CH=C×2), 8.10(2H, s, -NH-×2). ESI-MS *m/z*: 441.1 $(M+1)^+$, calcd for $C_{24}H_{28}N_2O_6$: 440.29.

(E)-N-(4-Chlorobenzyl)-3-(2,4-dimethoxyphenyl)acrylamide(2j): Yellow powder, 78.4% yield, mp 171.4-173.1°C. ^{1}H-NMR ($CDCl_3$): δ (ppm) 3.82 (3H, s, Ar-$OCH_3{}^4$), 3.84 (3H, s, Ar-$OCH_3{}^2$), 4.52(2H, d, J = 5.4 Hz, Ar-CH_2), 6.44 (1H, d, J = 15.6 Hz, =CH-C=O), 6.47 (1H, s, Ar-H^3), 6.49 (1H, d, J = 8.4 Hz, Ar-H^5), 7.25 (2H, d, J = 7.8 Hz, Ar^2-$H^{2,6}$), 7.29 (2H, d, J = 7.8 Hz, Ar^2-$H^{3,5}$), 7.38 (1H, d, J = 8.4 Hz, Ar-H^6), 7.82 (1H, d, J = 15.6 Hz, Ar-CH=C). ESI-MS *m/z*: 332.1 $(M+1)^+$, calcd for $C_{18}H_{18}ClNO_3$: 331.79.

(2E,2'E)-N,N'-(Hexane-1,6-diyl)bis(3-(2,4-dimethoxyphenyl)acrylamide)(2k): Yellow powder, 43.4% yield, mp 203.7-205.3°C. ^{1}H-NMR (DMSO): δ (ppm) 1.29 (4H, m, -N-C-C-CH_2×2), 1.43(4H, m, -N-C-CH_2×2), 3.14(4H, m, -N-CH_2×2), 3.80 (6H, s, Ar-$OCH_3{}^4$×2), 3.83 (6H, s, Ar-$OCH_3{}^2$×2), 6.51 (2H, d, J = 15.6 Hz, =CH-C=O×2), 6.56 (2H, d, J = 8.4 Hz, Ar-H^5×2), 6.59 (2H, s, Ar-H^3×2), 7.43 (2H, d, J = 8.4 Hz, Ar-H^6×2) , 7.55 (2H, d, J = 15.6 Hz, Ar-CH=C×2), 8.10(2H, t, J = 5.4 Hz,-NH-×2). ESI-MS *m/z*: 497.2 $(M+1)^+$, calcd for $C_{28}H_{36}N_2O_6$: 496.60.

(E)-N-Benzyl-3-(4-hydroxy-3-methoxyphenyl)acrylamide(3c) : **:** Yellow powder, 70.1% yield, mp 88.9-90.2°C. ^{1}H-NMR ($CDCl_3$): δ (ppm) 3.89 (3H, s, Ar-OCH_3), 4.57 (2H, d, J = 5.4 Hz, Ar-CH_2), 5.93 (1H, br.s, Ar-OH), 6.27 (1H, d, J = 15.6 Hz, =CH-C=O), 6.89 (1H, d, J = 8.4 Hz, Ar-H^5), 6.97 (1H, d, J = 1.8Hz, Ar-H^2), 7.05 (1H, dd, J_1 = 8.4 Hz, J_2 = 1.8 Hz, Ar-H^6), 7.28-7.35 (5H, m, Ar-H×5), 7.58 (1H, d, J = 15.6 Hz, Ar-CH=C). ESI-MS *m/z*: 284.1 $(M+1)^+$, 306.1 $(M+Na)^+$, calcd for $C_{17}H_{17}NO_3$: 283.32.

(E)-N-(3,4-Dimethoxybenzyl)-3-(4-hydroxy-3-methoxyphenyl)acrylamide(3f): Yellow powder, 68.4% yield, mp 63.7-65.9°C. ^{1}H-NMR ($CDCl_3$): δ (ppm) 3.80 (3H, s, Ar^2-$OCH_3{}^4$), 3.84 (3H, s, Ar^2-$OCH_3{}^3$), 3.88 (3H, s, Ar-OCH_3), 4.49 (2H, d, J = 6.0 Hz, Ar-CH_2), 6.13 (1H, br.s, Ar-OH), 6.29 (1H, d, J = 15.6 Hz, =CH-C=O), 6.79 (1H, d, J = 9.0 Hz, Ar^2-H^5), 6.84 (1H, d,

J = 9.0 Hz, Ar^2-H^6), 6.85 (1H, s, Ar^2-H^2), 6.88 (1H, d, J = 8.4 Hz, Ar-H^5), 6.96 (1H, d, J = 1.2 Hz, Ar-H^2), 7.02 (1H, dd, J_1 = 8.4 Hz, J_2 = 1.2 Hz, Ar-H^6), 7.57 (1H, d, J = 15.6 Hz, Ar-CH=C). ESI-MS *m/z*: 344.3 $(M+1)^+$, 366.2 $(M+Na)^+$, calcd for $C_{19}H_{21}NO_5$: 343.37.

(E)-N-(4-Fluorobenzyl)-3-(4-hydroxy-3-methoxyphenyl)acrylamide(3h): Yellow powder, 73.2% yield, mp 65.0-66.7°C. ^{1}H-NMR ($CDCl_3$): δ (ppm) 3.86 (3H, s, Ar-OCH_3), 4.51 (2H, d, J = 6.0 Hz, Ar-CH_2), 6.12 (1H, br.s, Ar-OH), 6.29 (1H, d, J = 15.6 Hz, =CH-C=O), 6.88 (1H, d, J = 8.4 Hz, Ar-H^5), 6.95 (1H, d, J = 1.2 Hz, Ar-H^2), 6.98 (1H, dd, J_1 = 8.4 Hz, J_2 = 1.2 Hz, Ar-H^6), 7.01-7.03 (2H, m, Ar^2-$H^{3,5}$), 7.26-7.28 (2H, m, Ar^2-$H^{2,6}$),7.57 (1H, d, J = 15.6 Hz, Ar-CH=C). ESI-MS *m/z*: 302.2 $(M+1)^+$, 324.1 $(M+Na)^+$, calcd for $C_{17}H_{16}FNO_3$: 301.31.

(E)-N-(4-Chlorobenzyl)-3-(4-hydroxy-3-methoxyphenyl)acrylamide(3j): Yellow powder, 79.0% yield, mp 58.7-60.3°C. ^{1}H-NMR ($CDCl_3$): δ (ppm) 3.86 (3H, s, Ar-OCH_3), 4.51 (2H, d, J = 6.0 Hz, Ar-CH_2), 6.12 (1H, br.s, Ar-OH), 6.29 (1H, d, J = 15.6 Hz, =CH-C=O), 6.88 (1H, d, J = 8.4 Hz, Ar-H^5), 6.95 (1H, d, J = 1.8 Hz, Ar-H^2), 7.03 (1H, dd, J_1 = 8.4 Hz, J_2 = 1.8 Hz, Ar-H^6), 7.23 (2H, d, J = 8.4 Hz, Ar^2-$H^{2,6}$), 7.27 (2H, d, J = 8.4 Hz, Ar^2-$H^{3,5}$), 7.57 (1H, d, J = 15.6 Hz, Ar-CH=C). ESI-MS *m/z*: 318.1 $(M+1)^+$, calcd for $C_{17}H_{16}ClNO_3$: 317.77.

(2E,2'E)-N,N'-(Hexane-1,6-diyl)bis(3-(4-hydroxy-3-methoxyphenyl)acrylamide)(3k): Yellow powder, 24.7% yield, mp 214.9-215.9°C. ^{1}H-NMR (DMSO): δ (ppm) 1.30 (4H, m, -N-C-C-CH_2×2), 1.44 (4H, m, -N-C-CH_2×2), 3.15 (4H, m, -N-CH_2×2), 5.95 (1H, br.s, Ar-OH), 6.50 (2H, d, J = 15.6 Hz, =CH-C=O×2), 6.88 (2H, d, J = 8.4 Hz, Ar-H^5×2), 6.96 (2H, d, J = 1.8 Hz, Ar-H^2×2), 7.03 (2H, dd, J_1 = 8.4 Hz, J_2 = 1.8 Hz,, Ar-H^6×2), 7.54 (2H, d, J = 15.6 Hz, Ar-CH=C×2), 8.03(2H, t, J = 5.4 Hz,-NH-×2). ESI-MS *m/z*: 469.1 $(M+1)^+$, 491.1 $(M+Na)^+$, calcd for $C_{26}H_{32}N_2O_6$: 468.54.

Animals

C57BL/6 (B6) mice weighing 18-22 g were obtained from the Animal Center of Wenzhou Medical University (Wenzhou, China). Animals were housed at a constant room temperature with a 12:12 hour light-dark cycle, and fed with a standard rodent diet and water. The animals

were acclimatized to the laboratory for at least 7 days before use in experiments. Protocols involving the use of animals were approved by the Wenzhou Medical University Animal Policy and Welfare Committee (Approval documents: 2013/APWC/0361).

Cells and treatment

Mouse RAW 264.7 macrophages were obtained from the American Type Culture Collection (ATCC, USA). Mouse primary peritoneal macrophages (MPMs) were prepared and cultured from C57BL/6 mice using the method described in our previous paper[18]. Both RAW 264.7 macrophages and MPMs were incubated in DMEM media (Gibco) supplemented with 10% FBS,100 U/ml penicillin, and 100 mg/ml streptomycin at 37 ºC with 5% CO_2. Compounds were added into cell cultural medium in DMSO solution with the final concentration of DMSO is 0.1%.

Determination of TNF-α and IL-6

After treatment of cells with compounds and LPS or Pam3CK, the TNF-α and IL-6 levels in media were determined with an enzyme-linked immunosorbent assay (ELISA) kit (BioScience, San Diego, CA) according to the manufacturer's instructions. The total amount of the inflammatory factor in the media was normalized to the total protein quantity of the viable cell pellets.

Real-time quantitative PCR

Cells were homogenized in TRIZOL kit (Invitrogen, Carlsbad, CA) for extraction of RNA according to each manufacturer's protocol. Both reverse transcription and quantitative PCR were carried out using a two-step M-MLV Platinum SYBR Green qPCR SuperMix-UDG kit (Invitrogen, Carlsbad, CA). Eppendorf Mastercycler ep realplex detection system (Eppendorf, Hamburg, Germany) were used for q-PCR analysis. The primers of genes including TNF-α, IL-6, PGES, IL-1β, COX-2, and β-actin were synthesized by Invitrogen. The primer sequences used are shown in Table S2. The amount of each gene was determined and normalized by the amount of β-actin.

Western Immunoblot analysis

The treated cells were collected and lysated, then 30 μg of the whole cell lysates were separated by 10% sodium dodecyl sulfate-polyacrylamide gel electrophoresis and electrotransferred to a nitrocellulose membrane. Each membrane was preincubated for 1 h at room temperature in Tris-buffered saline, pH 7.6, containing 0.05% tween-20 and 5% non-fat milk. Each nitrocellulose membrane was incubated with specific antibodies against p-p38, p38, p-JNK, JNK, p-ERK, ERK, IκB, or β-Actin (Santa Cruz, CA). Immunoreactive bands were then detected by incubating with secondary antibody conjugated with horseradish peroxidase and visualized using enhanced chemiluminescence reagents (Bio-Rad, Hercules, CA).

Assay of cellular NF-κB p-65 translocation

The cells were immunofluorescence-labeled according to the manufacturer's instructions using a Cellular NF-κB p-65 Translocation Kit (Beyotime Biotech, Nantong, China). P65 protein and nuclei fluoresce red and blue, respectively, and can be simultaneously viewed by fluorescence microscope (Nikon, Tokyo, Japan) at an excitation wavelength of 350 nm for DAPI, and 540 nm for Cy3. To create a two-color image, the red and blue images were overlaid, producing purple fluorescence in areas of co-localization.

Docking of 2i to the MD-2 structural model

In order to get further insight into the interactions mode between compound 2i and MD-2, flexible ligand rigid protein docking was performed using AutoDock version 4.2. The crystal structure of human MD-2-lipid IVa complex (PDB code 2E59) was derived from Protein Data Bank as the receptor in current docking model. The AutoDock Tools version 1.5.6 package was employed to generate the docking input files and to analyze the docking results. A grid box size of 60×60×60 points with a spacing of 0.375 Å between the grid points was implemented and covered almost the entire protein-binding site. The affinity maps of MD-2 were calculated using AutoGrid. One hundred Lamarckian Genetic Algorithm runs with default parameter settings were performed. The interactions of complex protein-ligand conformations hydrogen bonds and bond lengths were analyzed

Fluorescence measurements of bis-ANS dispalcment

Fluorescence measurements were performed with a spectraMax M5 (Molecular Devices, Sunnyvale, CA). All measurements were done at 25 ℃ in a 1 cm path-length quartz cuvette. Briefly, 1,1'-Bis(anilino)-4,4'-bis(naphthalene)-8,8'-disulfonate (bis-ANS, 5 μM) and rhMD-2 protein (5 nM) were mixed in PBS (pH 7.4) and incubated to reach stable relative fluorescence units (RFUs) emitted at 430–590 nm under excitation at 385 nm. Non-fluorescent 2i (at 2.5, 5, 10, 20, 40 μM) was then treated for 5 min, and followed by measuring relative fluorescence units (RFUs) emitted at 430-590 nm.

Surface Plasmon Resonance (SPR) Analysis

The binding affinity of 2i was determined using a ProteOn XPR36 Protein Interaction Array system (Bio-Rad Laboratories, Hercules, CA) with a HTE sensor chip(ProteOn™, #176-5033). Briefly, MD-2 and TLR4 protein (in acetate acid buffer pH 5.5) was loaded to the sensors which activated with 10 mM $NiSO_4$. And the 2i samples (at 100, 50, 25, 12.5 and 6.25 μM) were prepared with runing buffer (PBS, 0.1% SDS, 5% DMSO, and 0.05% Tween-20). Sensor and sample plate were placed on the instrument. The 2i samples were then captured in flow cells 1, leaving the second flow cell as a blank. Five concentrations were injected simultaneously at a flow rate of 30 μM /min for 120 s of association phase, followed with 120 s of dissociation phase at 25 ℃. The final graphs were obtained by subtracting blank sensorgrams from the duplex or quadruplex sensorgrams. Data were analyzed with ProteOn manager software. KD was calculated by global fitting of the kinetic data from various concentrations of 2i using 1:1 Langmuir binding model.

In vitro assay for LPS binding to MD2 (ELISA)

The MD-2 antibody was coated to 96-well at 4 ℃ overnight. RhMD-2, MD-2^{R90A} and MD-2^{Y102A} (4 μg/mL) in 10 mM Tris-HCl buffer was added to the pre-coated plate for 1.5 h at room temperature. After washing with PBST, biotin-labeled LPS was added to the plate with or without the presence of 2i (1 μM). Biotin-LPS binding to MD-2 was determined by ELISA, representing as absorbance values at 450 nm (A450). Data are mean values (±SD) of 3 separate experiments, each performed in duplication. *$P<0.05$, **$P<0.01$ vs. buffer alone-added group.

Flow Cytometric Analysis

Cellular binding of fluorescein isothiocyanate-labeled LPS (LPS-FITC, from E.coli 055:B5, Sigma, St. Louis, MO) was measured as described previously[29]. Briefly, HUVEC304 cells (1×10^5) were incubated with LPS-FITC (50 μg/mL) for 30 min with or without the presence of 2i. After washing, the cells with bound LPS-FITC were analyzed by flow cytometry.

Immunoprecipitation

Cells or mouse lung tissues were lysed by an extraction buffer (containing mammalian protein extraction reagent supplemented with protease and phosphatase inhibitor cocktails) and centrifuged at 12,000 rpm for 10 min at 4 ℃. Sufficient amount of MD-2 antibody was added into 400 μg proteins and gently rotated at 4 ℃ overnight. The immunocomplex were collected with protein A+G agarose (Beyotime Biotech, Nantong, China) and the precipitates were washed four times with ice-cold PBS. Then, proteins were released by boiling in sample buffer, followed by Western blot analysis as described above.

LPS-induced inflammatory mortality in B6 mice

Compound 2i was firstly dissolved with macrogol 15 hydroxystearate (a nonionic solubilizer for injection, from BASF [Ludwigshafen, Germany]) with or without medium-chain triglycerides (MCT, from BASF) in a water bath at 37°C. The concentration of 2i was 2 mg/mL. The concentration of solubilizer was 5%–10%, and MCT 0.5%–2.0% in final solution. For the vehicle, the mixture of solubilizer and MCT was prepared at 10% and 2%, respectively. Male C57BL/6 mice weighing 18–22 g were treated with 2i solution (200 μL, 10 mg/kg) by intravenous injection 15 minutes before the intraperitoneal injection of LPS (20 mg/kg). Control animals received a similar volume (200 μL) of vehicle. Bodyweight change and mortality were recorded for 7 days.

LPS-induced ALI

Male B6 mice were randomly divided into three groups, designated control (n = 6), LPS (n = 6) and 2i+LPS (n = 6). Prior to intratracheal injection of LPS (10 mg/kg), the mice were

treated orally with 2i at a dosage of 20 mg/kg for one week. Mice were then euthanized with ketamine 6 hours after LPS induction. The chest cavity of each animal was carefully opened and the collection of bronchoalveolar lavage fluid (BALF) was performed.

BALF analysis

The collected BALF was centrifuged at 1000 rpm for 10 min at 4 °C, the supernatant was used for protein concentration detection and subsequent cytokine determinations. The precipitation was resuspended using 50 μL physiological saline. The total number of cells on BALF was detected by cell counting instrument. The number of neutrophils on BALF was examined using Wright-Gimesa stain.

Lung Wet/Dry ratio

To observe the pulmonary edema, the lung wet/dry weight ratio was calculated. After the middle lobe of right lung was collected, the wet weight was recorded. Lung were then heated in a thermostatic oven at 65 °C for 72 h and weighed to determine the baseline lung dry mass levels.

Histopathological study

The superior lobe of right lung was collected and fixed in 4% paraformaldehyde, then embedded in paraffin and cut into 5 μm sections. The sections were stained with hematoxylin and eosin using standard protocol for light microscopy examination.

Immunohistochemistry

Tissue sections (5 μm thickness) were prepared, deparaffinized in xylene, and hydrated using an ethanol gradient. Pressure-cooker was used for antigen retrieval. After treatment with 30% of hydrogen peroxide, all the sections were blocked in 5% bovine serum albumin (BSA) and incubated with primary Anti-CD68 antibody for overnight at 4 °C. The slides were then incubated with HRP-labeled secondary antibody for 10 min. After the sections were stained with 3,3-diaminobenzidine tetrahydrochloride (DAB), the slides were evaluated under microscope.

Statistical analysis

The results are presented as means ± SD. The statistical significance of differences between groups was obtained by the student's t test or ANOVA multiple comparisons in GraphPad Pro5.0 (*GraphPad, San Diego, CA*). P values less than 0.05 ($p<0.05$) were considered indicative of significance. All experiments were repeated at least three times.

Acknowledgement

Financial support was provided by the National Natural Science Foundation of China (81472307, 21272179, and 81503123), and Natural Science Funding of Zhejiang Province (LY14C050004, LQ14H310003, and LQ15H120005).

Author Information Notes

Corresponding Author

wzmcliangguang@163.com; Tel: (+86)-577-86699396

Notes

The authors declare no competing financial interest.

Associated Content

Supporting Information. Additional experiments, Table S1-S2 and Figure S1-S10.

List of nonstandard abbreviations and acronyms

MD2: Myeloid Differentiation 2; LPS: Lipopolysaccharides;TLR4: Toll-like Receptor 4; ALI: Acute Lung Injury; CD14: Cluster of Differentiation 14; MAPKs: Mitogen-Activated Protein Kinases; NF-κB: Nuclear Factor Kappa-light-chain-enhancer of activated B cells; EDC-HCl: 1-(3-Dimethylaminopropyl)-3-ethylcarbodiimide hydrochloride; TNF–α: Tumor Necrosis Factor–α; HOBT: N-hydroxybenzotriazole; MPMs: Mouse Primary Peritoneal Macrophages; IL-6: Interleukin-6; SAR: Structure-Activity Relationship; IL-1β: Interleukin-1β; PGE: Prostaglandin E; COX-2: Cyclo-Oxygen-ase 2; JNK: c-Jun N-terminal Kinase; ERK: Extracellular Regulated protein Kinases; IκB: Inhibitor of NF-Kb; FITC: Fluorescein isothiocyanate isomer I; BALF: Bronchoalveolar lavage fluid; MPO: Myeloperoxidase

References

(1) Opal, S. M.; Laterre, P.-F.; Francois, B.; LaRosa, S. P.; Angus, D. C.; Mira, J.-P.; Wittebole, X.; Dugernier, T.; Perrotin, D.; Tidswell, M.; Jauregui, L.; Krell, K.; Pachl, J.; Takahashi, T.; Peckelsen, C.; Cordasco, E.; Chang, CS.; Oeyen, S.; Aikawa, N.; Maruyama, T.; Schein, R.; Kalil, AC.; Van, Nuffelen, M.; Lynn, M.; Rossignol, DP.; Gogate, J.; Roberts, MB.; Wheeler, JL.; Vincent, JL. Effect of eritoran, an antagonist of MD2-TLR4, on mortality in patients with severe sepsis: the ACCESS randomized trial. *JAMA* **2013,** *309*, 1154-1162.

(2) Letsiou, E.; Sammani, S.; Naureckas, P.; Jacobson, J.; Garcia, J.; Dudek, S.; Rizzo, A. Imatinib inhibits LPS-induced endothelial dysfunction and acute lung injury. *Am. J. Respir. Crit. Care Med.* **2014,** *189*, A2207.

(3) Viladés, C.; Escoté, X.; López-Dupla, M.; Martinez, E.; Domingo, P.; Asensi, V.; Leal, M.; Peraire, J.; Inza, M.-I.; Arnedo, M.; Gutiérrez, M.; Valle-Garay, E.; Ferrando-Martinez, S.; Olona, M.; Alba, V.; Sirvent, JJ.; GateII, JM.; Vidal, F. Involvement of the LPS-LPB-CD14-MD2-TLR4 inflammation pathway in HIV-1/HAART-associated lipodystrophy syndrome (HALS). *J. Antimicrob. Chemother.* **2014,** *69*, 1653-1659.

(4) Lu, Y.-C.; Yeh, W.-C.; Ohashi, P. S. LPS/TLR4 signal transduction pathway. *Cytokine* **2008,** *42*, 145-151.

(5) Yamamoto, M.; Akira, S. Lipid A receptor TLR4-mediated signaling pathways. In *Lipid A in Cancer Therapy;* Springer New York: 2010; pp 59-68.

(6) Gaieski, D. F.; Goyal, M. What is sepsis? What is severe sepsis? What is septic shock? Searching for objective definitions among the winds of doctrines and wild theories. *Expert Rev. Anti-Infect. Ther.* **2013,** *11*, 867.

(7) Balk, R. A. Systemic inflammatory response syndrome (SIRS) Where did it come from and is it still relevant today? *Virulence* **2014,** *5*, 20-26.

(8) Levitt, J. E.; Matthay, M. A. Clinical review: Early treatment of acute lung injury-paradigm shift toward prevention and treatment prior to respiratory failure. *Crit. Care* **2012,** *16*, 223.

(9) Hyakushima, N.; Mitsuzawa, H.; Nishitani, C.; Sano, H.; Kuronuma, K.; Konishi, M.; Himi, T.; Miyake, K.; Kuroki, Y. Interaction of soluble form of recombinant extracellular TLR4 domain with MD-2 enables lipopolysaccharide binding and attenuates TLR4-mediated signaling. *J. Immunol.* **2004,** *173*, 6949-6954.

(10) Nagai, Y.; Akashi, S.; Nagafuku, M.; Ogata, M.; Iwakura, Y.; Akira, S.; Kitamura, T.; Kosugi, A.; Kimoto, M.; Miyake, K. Essential role of MD-2 in LPS responsiveness and TLR4 distribution. *Nat. Immunol.* **2002,** *3*, 667-672.

(11) De, P.; Baltas, M.; Bedos-Belval, F. Cinnamic acid derivatives as anticancer agents-a review. *Curr. Med. Chem.* **2011,** *18*, 1672-1703.

(12) Sova, M. Antioxidant and antimicrobial activities of cinnamic acid derivatives. *Mini-Rev. Med. Chem.* **2012,** *12*, 749-767.

(13) Giles, F.; Fischer, T.; Cortes, J.; Garcia-Manero, G.; Beck, J.; Ravandi, F.; Masson, E.; Rae, P.; Laird, G.; Sharma, S.; Kantarjian, H.; Dugan, M.; Albitar, M.; Bhalla, K. A phase I study of intravenous LBH589, a novel cinnamic hydroxamic acid analogue histone deacetylase inhibitor, in patients with refractory hematologic malignancies. *Clin. Cancer Res.* **2006,** *12*, 4628-4635.

(14) Gunia‐Krzyżak, A.; Pańczyk, K.; Waszkielewicz, A. M.; Marona, H. Cinnamamide derivatives for central and peripheral nervous system disorders—a review of structure–activity relationships. *ChemMedChem* **2015,** *10*, 1302-1325.

(15) Musso, D. L.; Cochran, F. R.; Kelley, J. L.; McLean, E. W.; Selph, J. L.; Rigdon, G. C.; Orr, G. F.; Davis, R. G.; Cooper, B. R.; Styles, V. L.; Thompson, JB.; Hall, WR. Indanylidenes. 1. Design and synthesis of (E)-2-(4, 6-difluoro-1-indanylidene) acetamide, a potent, centrally acting muscle relaxant with antiinflammatory and analgesic activity. *J. Med. Chem.* **2003,** *46*, 399-408.

(16) Matsui, T.; Ito, C.; Furukawa, H.; Okada, T.; Itoigawa, M. Lansiumamide B and SB-204900 isolated from Clausena lansium inhibit histamine and TNF-α release from RBL-2H3 cells. *Inflammation Res.* **2013,** *62*, 333-341.

(17) Palomba, M.; Pau, A.; Boatto, G.; Asproni, B.; Auzzas, L.; Cerri, R.; Arenare, L.; Filippelli, W.; Falcone, G.; Motola, G. Anti‐inflammatory and analgesic amides: new developments. *Arch. Pharm.* **2000,** *333*, 17-26.

(18) Wu, J.; Li, J.; Cai, Y.; Pan, Y.; Ye, F.; Zhang, Y.; Zhao, Y.; Yang, S.; Li, X.; Liang, G. Evaluation and discovery of novel synthetic chalcone derivatives as anti-inflammatory agents. *J. Med. Chem.* **2011,** *54*, 8110-8123.

(19) Yu, P.; Dong, L.; Zhang, Y.; Chen, W.; Xu, S.; Wang, Z.; Shan, X.; Zhou, J.; Liu, Z.; Liang, G. Design, synthesis and biological activity of novel asymmetric C66 analogs as anti-inflammatory agents for the treatment of acute lung injury. *Eur. J. Med. Chem.* **2015,** *94*, 436-446.

(20) Pastukhov, A. V.; Ropson, I. J. Fluorescent dyes as probes to study lipid-binding proteins. *Proteins* **2003,** *53*, 607-615.

(21) Mancek-Keber, M.; Jerala, R. Structural similarity between the hydrophobic fluorescent probe and lipid A as a ligand of MD-2. *FASEB J.* **2006,** *20*, 1836-1842.

(22) Bernard, G. R.; Wheeler, A. P.; Russell, J. A.; Schein, R.; Summer, W. R.; Steinberg, K. P.; Fulkerson, W. J.; Wright, P. E.; Christman, B. W.; Dupont, W. D.; Higgins, SB.; Swindell, BB. The effects of ibuprofen on the physiology and survival of patients with sepsis. *N. Engl. J. Med.* **1997,** *336*, 912-918.

(23) Watanabe, T.; Higuchi, K.; Kobata, A.; Nishio, H.; Tanigawa, T.; Shiba, M.; Tominaga, K.; Fujiwara, Y.; Oshitani, N.; Asahara, T.; Nomoto, K.; Takeuchi, K.; Arakawa, T. Non-steroidal anti-inflammatory drug-induced small intestinal damage is Toll-like receptor 4 dependent. *Gut* **2008,** *57*, 181-187.

(24) Sharma, P. Cinnamic acid derivatives: A new chapter of various pharmacological activities. *J. Chem. Pharm. Res.* **2011,** *3*, 403-423.

(25) Hoskins, J. A. The occurrence, metabolism and toxicity of cinnamic acid and related compounds. *J. Appl. Toxicol.* **1984,** *4*, 283-292.

(26) Lomenick, B.; Hao, R.; Jonai, N.; Chin, R. M.; Aghajan, M.; Warburton, S.; Wang, J.; Wu, R. P.; Gomez, F.; Loo, J. A.; Wohlschlegel, JA.; Vondriska, TM.; Pelletier, J.; Herschman, HR.; Clardy, J.; Clarke, CF.; Huang J. Target identification using drug affinity responsive target stability (DARTS). *Proc. Natl. Acad. Sci.* **2009,** *106*, 21984-21989.

(27) Lomenick, B.; Olsen, R. W.; Huang, J. Identification of direct protein targets of small molecules. *ACS Chem. Biol.* **2010,** *6*, 34-46.

(28) Gradišar, H.; Keber, M. M.; Pristovšek, P.; Jerala, R. MD-2 as the target of curcumin in the inhibition of response to LPS. *J. Leukocyte Biol.* **2007,** *82*, 968-974.

(29) Roh, E.; Lee, H.-S.; Kwak, J.-A.; Hong, J. T.; Nam, S.-Y.; Jung, S.-H.; Lee, J. Y.; Kim, N. D.; Han, S.-B.; Kim, Y. MD-2 as the target of nonlipid chalcone in the inhibition of endotoxin

LPS-induced TLR4 activity. *J. Infect. Dis.* **2011,** *203*, 1012-1020.

(30) Peluso, M. R.; Miranda, C. L.; Hobbs, D. J.; Proteau, R. R.; Stevens, J. F. Xanthohumol and related prenylated flavonoids inhibit inflammatory cytokine production in LPS-activated THP-1 monocytes: structure-activity relationships and in silico binding to myeloid differentiation protein-2 (MD-2). *Planta Med.* **2010,** *76*, 1536-1543.

(31) Kim, S. Y.; Koo, J. E.; Seo, Y. J.; Tyagi, N.; Jeong, E.; Choi, J.; Lim, K. M.; Park, Z. Y.; Lee, J. Y. Suppression of Toll−like receptor 4 activation by caffeic acid phenethyl ester is mediated by interference of LPS binding to MD2. *Br. J. Pharmacol.* **2013,** *168*, 1933-1945.

(32) Park, S. H.; Kyeong, M. S.; Hwang, Y.; Ryu, S. Y.; Han, S.-B.; Kim, Y. Inhibition of LPS binding to MD-2 co-receptor for suppressing TLR4-mediated expression of inflammatory cytokine by 1-dehydro-10-gingerdione from dietary ginger. *Biochem. Biophys. Res. Commun.* **2012,** *419*, 735-740.

(33) Wang, Y.; Shan, X.; Chen, G.; Jiang, L.; Wang, Z.; Fang, Q.; Liu, X.; Wang, J.; Zhang, Y.; Wu, W.; Liang, G. MD‐2 as the target of a novel small molecule, L6H21, in the attenuation of LPS‐induced inflammatory response and sepsis. *Br. J. Pharmacol.* **2015,** *172*, 4391-4405.

(34) Wang, Y.; Shan, X.; Dai, Y.; Jiang, L.; Chen, G.; Zhang, Y.; Wang, Z.; Dong, L.; Wu, J.; Guo, G.; Liang, G. Curcumin analog L48H37 prevents Lipopolysaccharide-induced TLR4 signaling pathway activation and sepsis via targeting MD2. *J. Pharmacol. Exp. Ther.* **2015,** *353*, 539-550.

(35) Wang, Z.; Chen, G.; Chen, L.; Liu, X.; Fu, W.; Zhang, Y.; Li, C.; Liang, G.; Cai, Y. Insights into the binding mode of curcumin to MD-2: studies from molecular docking, molecular dynamics simulations and experimental assessments. *Mol. BioSyst.* **2015,** 11, 1933-1938.

(36) Kim, H. M.; Park, B. S.; Kim, J.-I.; Kim, S. E.; Lee, J.; Oh, S. C.; Enkhbayar, P.; Matsushima, N.; Lee, H.; Yoo, O. J.; Lee, JO. Crystal structure of the TLR4-MD-2 complex with bound endotoxin antagonist Eritoran. *Cell* **2007,** *130*, 906-917.

(37) Ohto, U.; Fukase, K.; Miyake, K.; Satow, Y. Crystal structures of human MD-2 and its complex with antiendotoxic lipid IVa. *Science* **2007,** *316*, 1632-1634.

(38) Resman, N.; Gradišar, H.; Vašl, J.; Keber, M. M.; Pristovšek, P.; Jerala, R. Taxanes inhibit human TLR4 signaling by binding to MD-2. *FEBS Lett.* **2008,** *582*, 3929-3934.

(39) Reinhart, K.; Glück, T.; Ligtenberg, J.; Tschaikowsky, K.; Bruining, A.; Bakker, J.; Opal, S.; Moldawer, L. L.; Axtelle, T.; Turner, T.; Souza, S.; Pribble, J. CD14 receptor occupancy in severe sepsis: Results of a phase I clinical trial with a recombinant chimeric CD14 monoclonal antibody (IC14)*. *Crit. Care Med.* **2004,** *32*, 1100-1108.

(40) Schuller, D.; Schuster, D. P. Fluid-management strategies in acute lung injury. *N. Engl. J. Med.* **2006,** *355*, 1175.

(41) Wheeler, A. P.; Bernard, G. R. Acute lung injury and the acute respiratory distress syndrome: a clinical review. *Lancet* **2007,** *369*, 1553-1564.

(42) Hađina, S.; Weiss, J. P.; McCray Jr, P. B.; Kulhankova, K.; Thorne, P. S. MD-2–dependent pulmonary immune responses to inhaled lipooligosaccharides: Effect of acylation state. *Am. J. Respir. Cell Mol. Biol.* **2008,** *38*, 647-654.

Figure Legends

Scheme 1. The structure of cinnamamides and the general synthesis of cinnamamides.

Table 1. Chemical structures of synthesized cinnamamides and their synthetic yields.

Figure 1. Inhibition of pro-inflammatory cytokines production by cinnamamide derivatives. (A) Effects of cinnamamides at 10μM on TNF-α production in LPS-stimulated MPMs. (B and C) Four active cinnamamides inhibited LPS-induced TNF-α and IL-6 release in a dose-dependent manner. After plating and 24 h of growth, MPMs were treated with LPS (0.5 μg/mL) in the presence of vehicle or synthesized analogues at indicated concentrations for further 24 h. Culture medium and proteins were collected. The TNF-α and IL-6 levels in medium were determined by ELISA. Data are expressed as fold change relative to control values (samples treated with LPS alone), mean ± SEM; n = 4. *p< 0.05 and **p< 0.01 vs. LPS alone-stimulated group.

Figure 2. The most active compound **2i** inhibit LPS-induced expression of inflammatory genes and activation of MAPK and NF-κB. (A) Chemical structure of **2i**. (B) MPMs were pretreated with vehicle or **2i** (10 μM) for 30 min followed by incubation with LPS (0.5 μg/mL) for 6 h. Expression of TNF-α, IL-6, IL-1β, COX-2 and PGES was quantified by quantitative PCR (qPCR) using specific primers and normalization against the housekeeping gene β-actin. (C, D, E and I) MPMs were pretreated with vehicle or **2i** (2.5, 5, or 10 μM) for 30 min followed by incubation with LPS (0.5 μg/mL) for 20 min. The protein levels of p-ERK, ERK, p-P38, P38, p-JNK, JNK, IκBα, and β-Actin were measured by western immunoblot analysis. For IκBα detection, ERK inhibitor PD98059 (PD, at 10μM) and p38 inhibitor SB239063 (SB, at 10μM) were used for comparison. (F, G and H) MPMs were pretreated with vehicle or **2i** (10 μM) for 30 min followed by incubation with LPS (0.5 μg/mL) for 1 h. Cells were subjected to fluorescence microscope (200×), displaying the NF-κB P65-stained with Cy3-labeled antibody by a pink color and the nuclei-stained with 4,6-diamidino-2-phenylindole by a blue color. Data are mean values (±SEM) of 3-5 separate experiments. *p< 0.05 and **p< 0.01 vs LPS

alone-stimulated group.

Figure 3. 2i act as a MD2 inhibitor. (A) Surface plasmon resonance (SPR) analysis showed that there is no direct interaction between **2i** and rhTLR4. (B) SPR analysis showed that **2i** directly binding to rhMD2 in a dose-dependent manner. (C) Fluorescence measurements showed that **2i** dose-dependently inhibited the binding of bis-ANS and rhMD-2. (D) Determination in ELISA system showed that **2i** inhibited the binding of Biotin-LPS to rhMD2. (E) Flow cytometry analysis showed that **2i** decreased the levels of LPS-FITC in cell surface in a dose-dependent manner. (F) Immunoprecipitation assay showed that **2i** pretreatment at 10μM significantly reduced the formation of TLR4-MD2 complex induced by 0.5 μg/mL LPS. (G and H) RAW264.7 macrophages were pretreated with vehicle control (0.1% DMSO), **2i** (5 or 10 μM), or TLR2 inhibitor CU-CPT22 (5 or 10 μM) for 2h followed by incubation with Pam3CK (0.1 μg/mL) for 12 h. The protein level of IL-6 (G) and TNF-α (H) in the culture medium was measured by ELISA and normalized to the total protein amount, respectively. Data are mean values (±SEM) of at least 3 separate experiments (**P<0.01).

Figure 4 2i binds MD2 via acting on Arg90 and Tyr102. (A) The molecular docking model of 2i with MD-2 protein (PDB code 2E59). (B and C) ELISA system and SPR analysis showed that 2i lost the inhibitory activity to rhMD-2^{R90A}. (D and E) ELISA system and SPR analysis also showed that 2i lost the inhibitory activity to rhMD-2^{Y102A}. Data are mean values (±SEM) of at least 3 separate experiments.

Figure 5 2i attenuates LPS-induced septic death in mice. C57BL/6 mice (n=9 per group) were i.v. injected with 10 mg/kg **2i** (in a water-soluble liposome formation) 15 min before i.p. injection of 20 mg/kg LPS. Survival rates (A) were recorded for 7 days after LPS injection (** P<0.01 vs LPS-treated group).

Figure 6 2i improved lung injury in LPS-induced septic mice. C57BL/6 mice (n=6 per group) Mice were orally administrated with **2i** (20 mg/kg) 15 min before intratracheal injection of LPS (10 mg/kg). Mice were killed at 6 h after LPS injection. (A) **2i** inhibit the increase of the protein

concentration in rat BALF. (B) **2i** suppressed LPS-induced lung edema. (C and D) Treatment with **2i** significantly reduced the numbers of total cells (C) and neutrophils (D) in BALF. (E) **2i** significantly decreased LPS-induced MPO activity in mice lung tissues. (F) hematoxylin and eosin (H&E) staining showed that **2i** attenuated LPS-induced pathological changes. (G) **2i** exhibited the inhibitory effect against macrophage infiltration. (H, I and J) **2i** inhibit LPS-induced mRNA expression of inflammatory cytokines including TNF-α, IL-6, and IL-1β in mice lung tissues. (K) Immunoprecipitation assay of lung tissue homogenates showed that **2i** significantly reduced the formation of TLR4-MD2 complex induced by LPS. (* $P<0.05$ vs LPS-treated group).

Figure 7 Illustration of the protection provided by **2i** against LPS-induced inflammation and sepsis via targeting MD2.

Table of Contents graphic

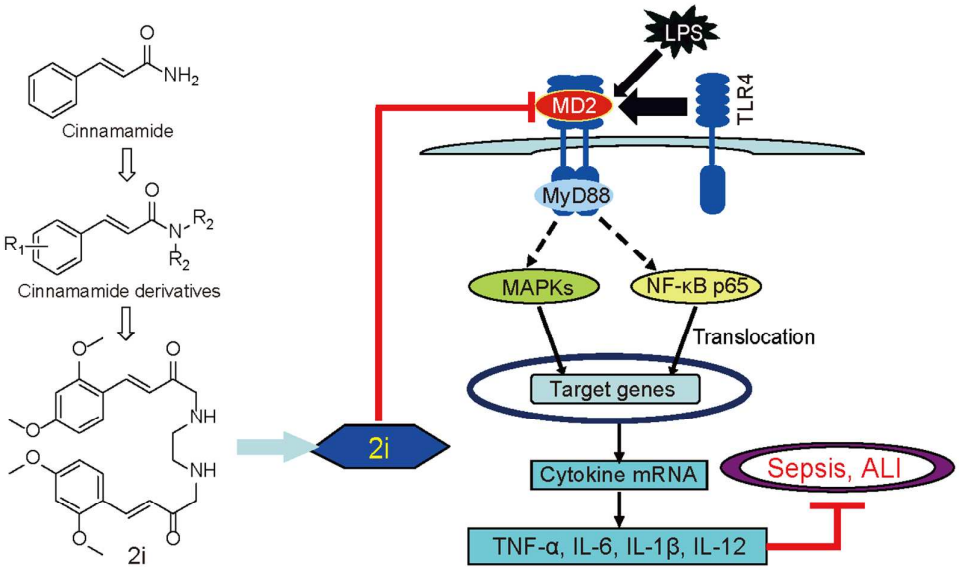

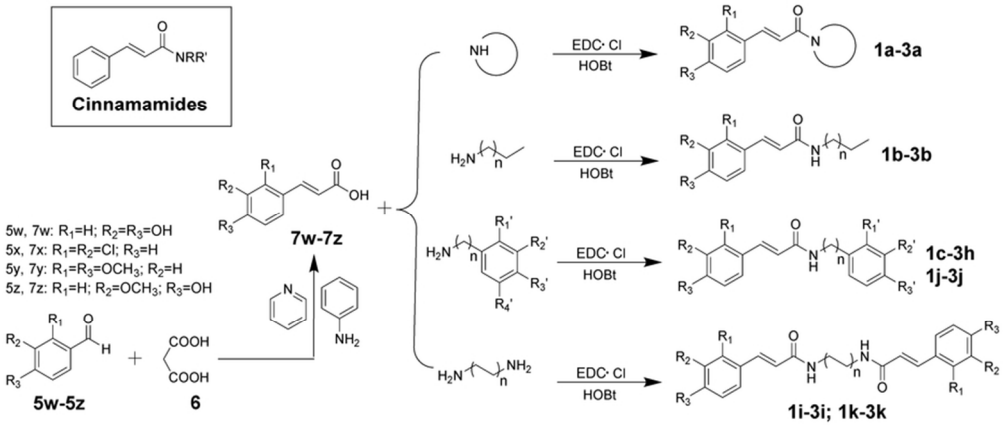

Scheme 1
78x33mm (300 x 300 DPI)

Table 1

Compound (yield) / R	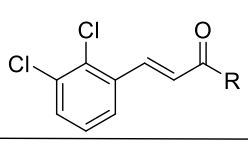	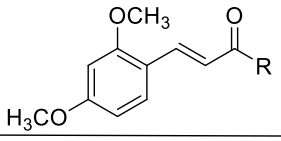	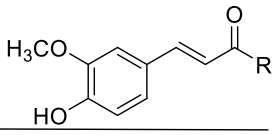
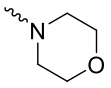	1a (85.3%)	2a (84.3%)	3a (76.2%)
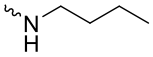	1b (83.2%)	2b (76.4%)	3b (71.1%)
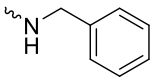	1c (79.6%)	2c (83.3%)	3c (70.1%)
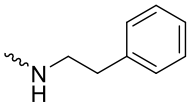	1d (82.1%)	2d (81.1%)	3d (80.2%)
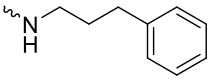	1e (79.6%)	2e (75.1%)	3e (70.3%)
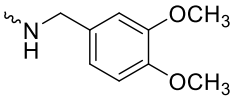	1f (83.5%)	2f (70.1%)	3f (68.4%)
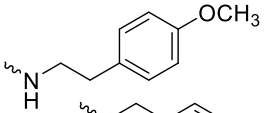	1g (79.6%)	2g (69.5%)	3g (73.6%)
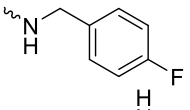	1h (73.3%)	2h (80.1%)	3h (73.2%)
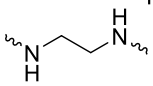	1i (54.3%)	2i (35.6%)	3i (22.7%)
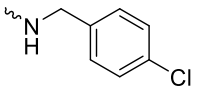	1j (76.2%)	2j (78.4%)	3j (79.0%)
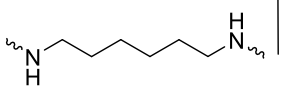	1k (44.5%)	2k (43.4%)	3k (24.7%)

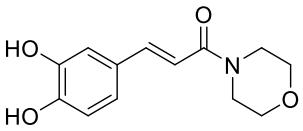 4a (79.8%)

Figure 1

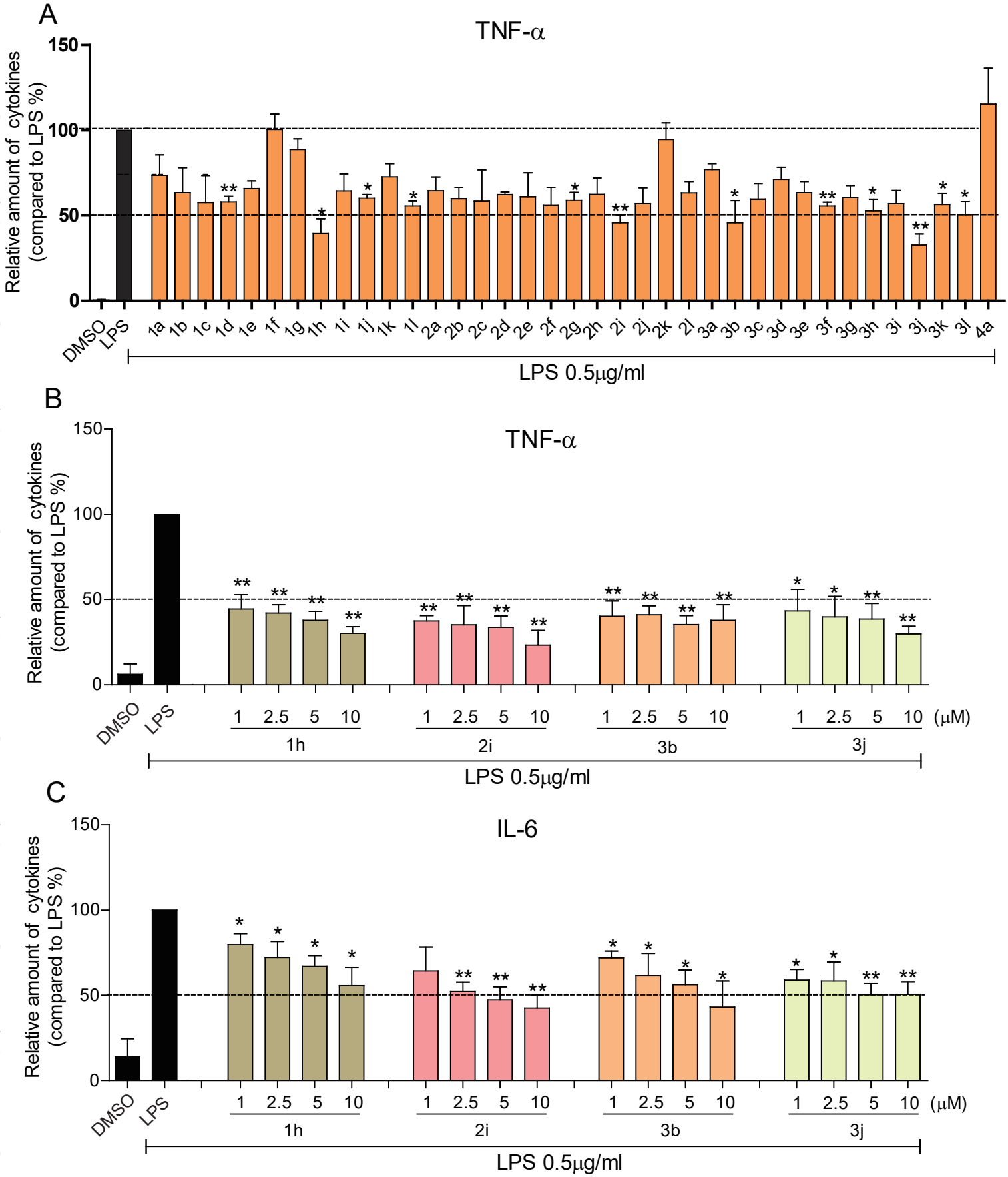
A
TNF-α
Relative amount of cytokines (compared to LPS %)
150
100
50
0
DMSO
LPS
1a 1b 1c 1d 1e 1f 1g 1h 1i 1j 1k 1l 2a 2b 2c 2d 2e 2f 2g 2h 2i 2j 2k 2l 3a 3b 3c 3d 3e 3f 3g 3h 3i 3j 3k 3l 4a
LPS 0.5μg/ml
B
TNF-α
Relative amount of cytokines (compared to LPS %)
150
100
50
0
DMSO
LPS
1 2.5 5 10 1 2.5 5 10 1 2.5 5 10 1 2.5 5 10 (μM)
1h
2i
3b
3j
LPS 0.5μg/ml
C
IL-6
Relative amount of cytokines (compared to LPS %)
150
100
50
0
DMSO
LPS
1 2.5 5 10 1 2.5 5 10 1 2.5 5 10 1 2.5 5 10 (μM)
1h
2i
3b
3j
LPS 0.5μg/ml

Figure 2

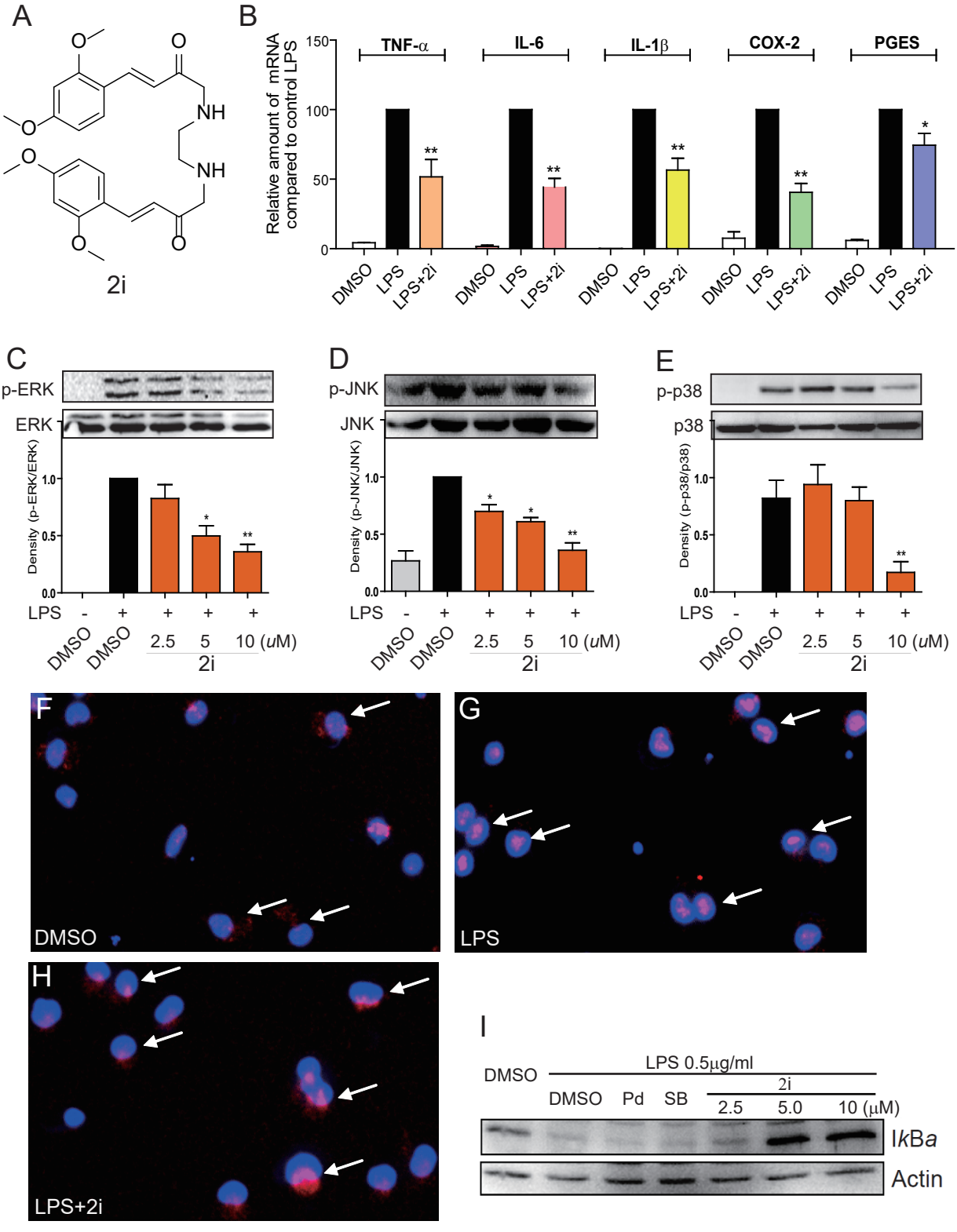
A
2i
B
Relative amount of mRNA compared to control LPS
TNF-α
IL-6
IL-1β
COX-2
PGES
DMSO
LPS
LPS+2i
C
p-ERK
ERK
Density (p-ERK/ERK)
D
p-JNK
JNK
Density (p-JNK/JNK)
E
p-p38
p38
Density (p-p38/p38)
LPS
2.5
5
10 (uM)
F
DMSO
G
LPS
H
LPS+2i
I
LPS 0.5μg/ml
Pd
SB
2.5
5.0
10 (μM)
IkBa
Actin

Figure 3

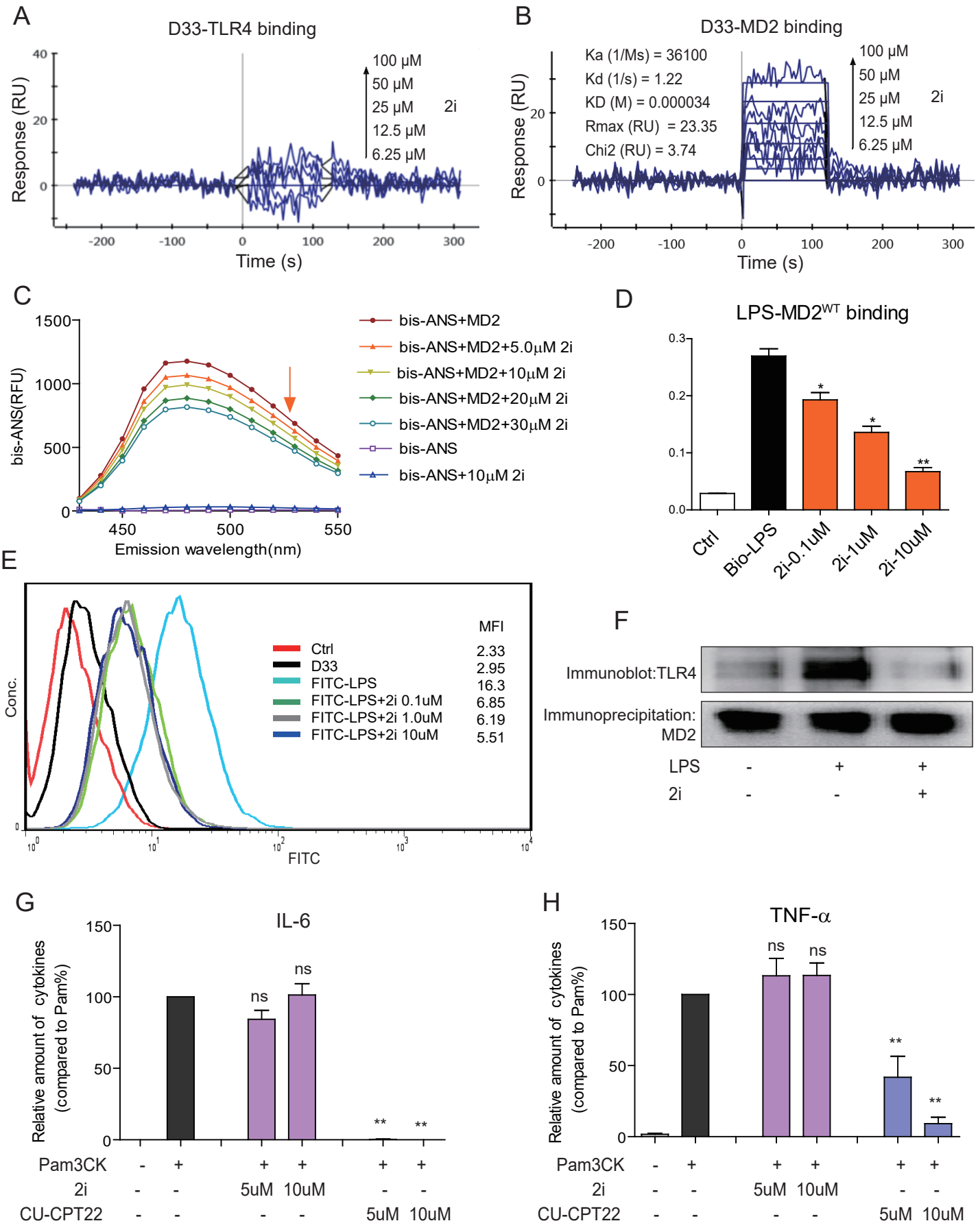
A
D33-TLR4 binding
Response (RU)
Time (s)
100 μM
50 μM
25 μM
12.5 μM
6.25 μM
2i
B
D33-MD2 binding
Ka (1/Ms) = 36100
Kd (1/s) = 1.22
KD (M) = 0.000034
Rmax (RU) = 23.35
Chi2 (RU) = 3.74
C
bis-ANS(RFU)
Emission wavelength(nm)
bis-ANS+MD2
bis-ANS+MD2+5.0μM 2i
bis-ANS+MD2+10μM 2i
bis-ANS+MD2+20μM 2i
bis-ANS+MD2+30μM 2i
bis-ANS
bis-ANS+10μM 2i
D
LPS-MD2WT binding
Ctrl
Bio-LPS
2i-0.1uM
2i-1uM
2i-10uM
E
Conc.
FITC
MFI
Ctrl 2.33
D33 2.95
FITC-LPS 16.3
FITC-LPS+2i 0.1uM 6.85
FITC-LPS+2i 1.0uM 6.19
FITC-LPS+2i 10uM 5.51
F
Immunoblot:TLR4
Immunoprecipitation: MD2
LPS
2i
G
IL-6
Relative amount of cytokines (compared to Pam%)
Pam3CK
2i
CU-CPT22
5uM
10uM
ns
H
TNF-α
Relative amount of cytokines (compared to Pam%)
Pam3CK
2i
CU-CPT22
5uM
10uM
ns

Figure 4

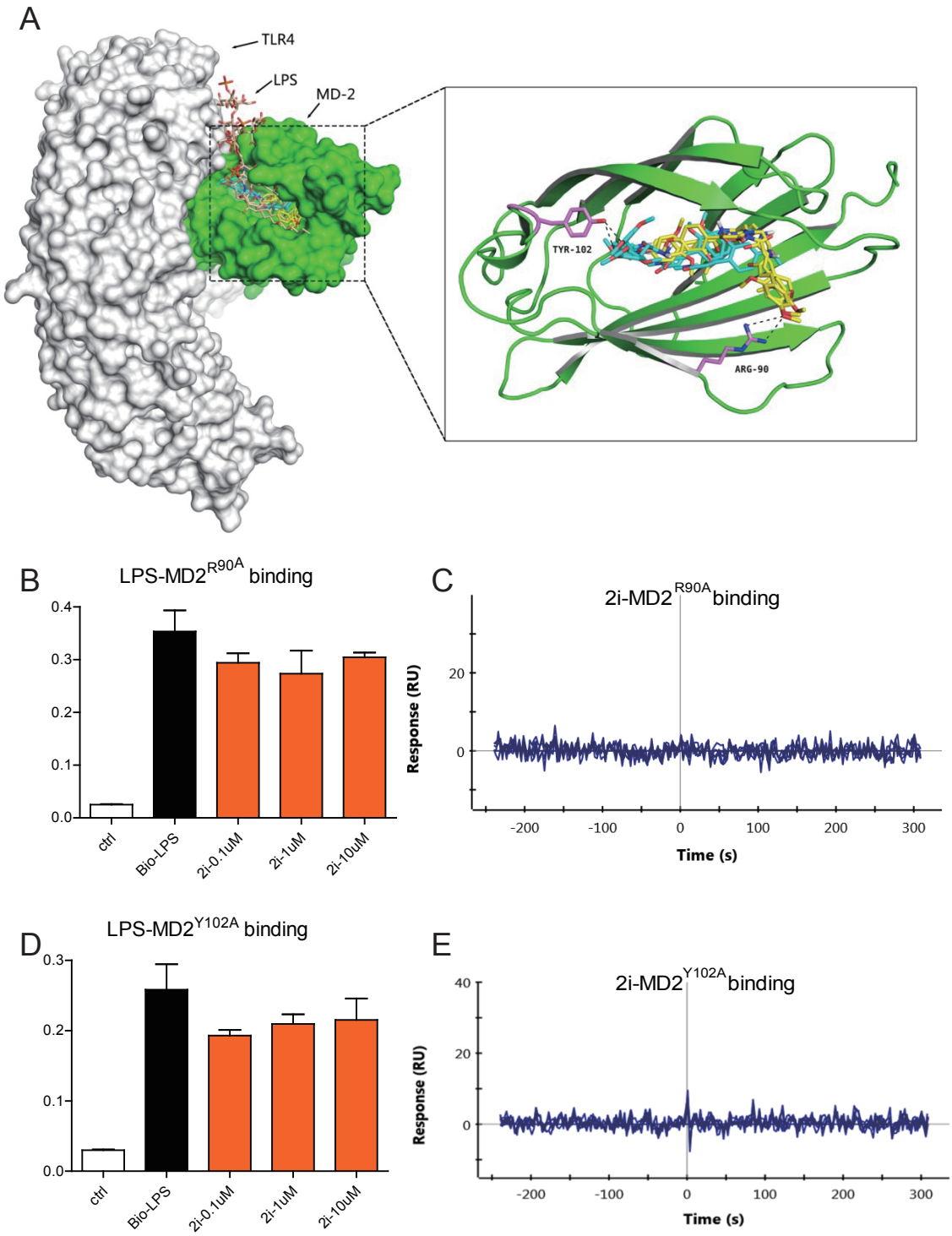
A
TLR4
LPS
MD-2
TYR-102
ARG-90
B
LPS-MD2R90A binding
0.4
0.3
0.2
0.1
0.0
ctrl
Bio-LPS
2i-0.1uM
2i-1uM
2i-10uM
C
2i-MD2R90A binding
Response (RU)
20
0
-200
-100
0
100
200
300
Time (s)
D
LPS-MD2Y102A binding
0.3
0.2
0.1
0.0
ctrl
Bio-LPS
2i-0.1uM
2i-1uM
2i-10uM
E
2i-MD2Y102A binding
Response (RU)
40
20
0
-200
-100
0
100
200
300
Time (s)

Figure 5

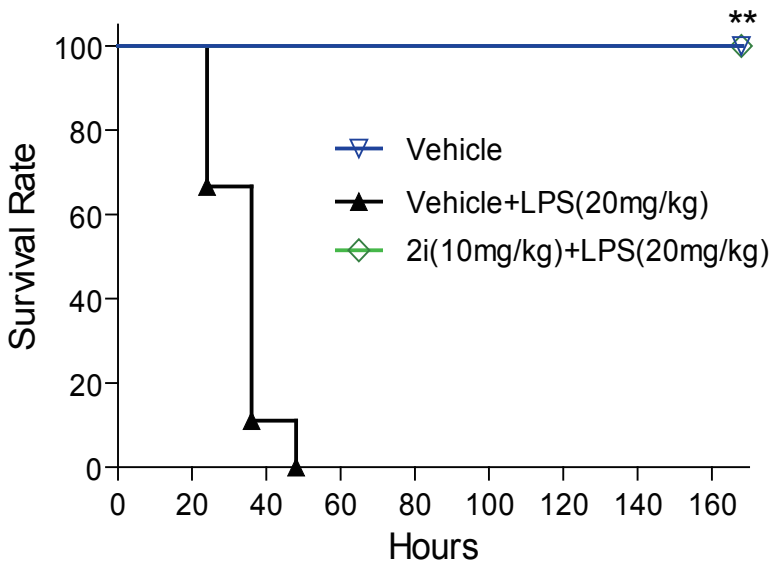
**
100
80
60
40
20
0
Survival Rate
0
20
40
60
80
100
120
140
160
Hours
Vehicle
Vehicle+LPS(20mg/kg)
2i(10mg/kg)+LPS(20mg/kg)

Figure 6

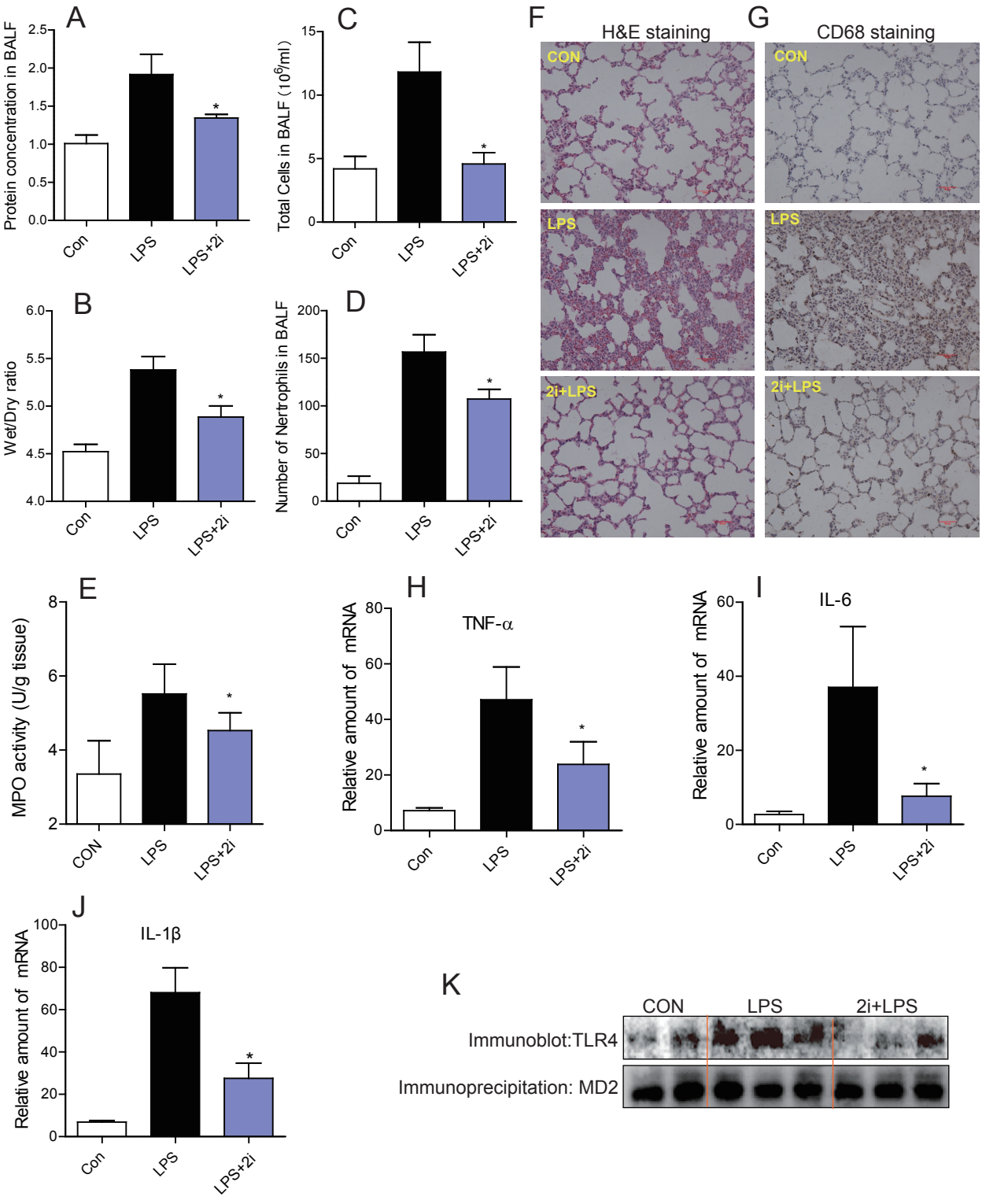
A
Protein concentration in BALF
2.5
2.0
1.5
1.0
0.5
0.0
Con
LPS
LPS+2i
C
Total Cells in BALF (10^6/ml)
15
10
5
0
B
Wet/Dry ratio
6.0
5.5
5.0
4.5
4.0
D
Number of Nertrophils in BALF
200
150
100
50
0
F
H&E staining
G
CD68 staining
CON
LPS
2i+LPS
E
MPO activity (U/g tissue)
8
6
4
2
H
TNF-α
Relative amount of mRNA
80
60
40
20
0
I
IL-6
60
40
20
0
J
IL-1β
100
80
60
40
20
0
K
CON
LPS
2i+LPS
Immunoblot:TLR4
Immunoprecipitation: MD2

Figure 7

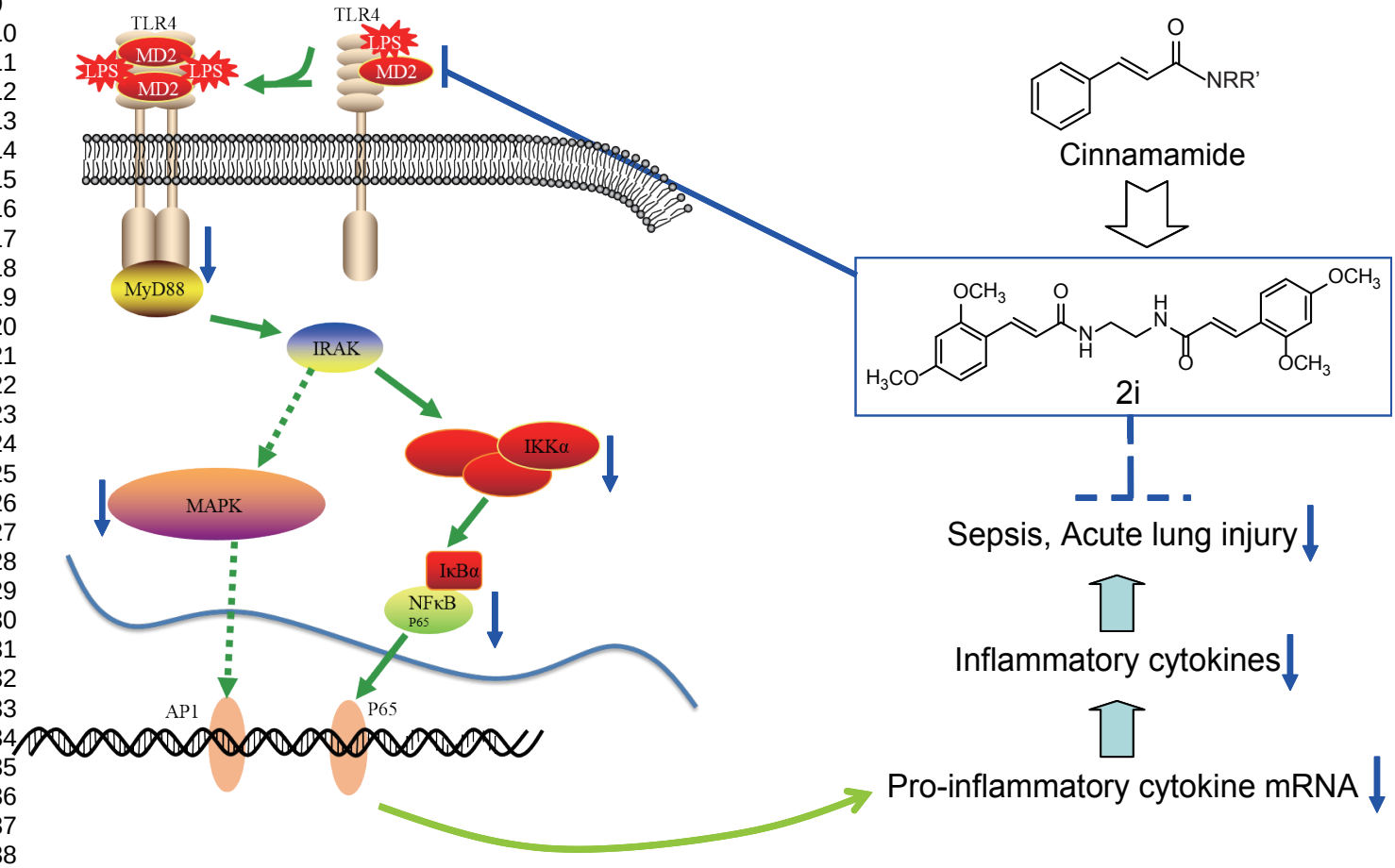
TLR4
TLR4
MD2
LPS
LPS
MD2
LPS
MD2
MyD88
IRAK
IKKα
MAPK
IκBα
NFκB
P65
AP1
P65
O
NRR'
Cinnamamide
OCH3
O
H
N
N
H
O
OCH3
H3CO
OCH3
2i
Sepsis, Acute lung injury
Inflammatory cytokines
Pro-inflammatory cytokine mRNA